

Electronic Supplementary Information

For the Manuscript Entitled

Chemosensors containing appended benzothiazole group(s): Selective binding of Cu²⁺ and Zn²⁺ ions by two related receptors

Deepak Bansal and Rajeev Gupta*

Department of Chemistry, University of Delhi, Delhi – 110 007

Index

1. Experimental Section.
2. Synthesis of Chemosensors.
3. Synthesis of Metal Complexes.
4. Physical Measurements.
5. Crystallography.
6. Fabrication of films and strips.

List of Figures

Figure S1. ¹H (top) and ¹³C NMR (bottom) spectra of chemosensor **2** in DMSO-d₆. * Represents the residual solvent peak.

Figure S2. ¹H (top) and ¹³C NMR (bottom) spectra of chemosensor **3** in DMSO-d₆. * Represents the residual solvent peak(s).

Figure S3. ¹H (top) and ¹³C NMR (bottom) spectra of chemosensor **4** in DMSO-d₆. * Represents the residual solvent peak(s).

Figure S4. (Top) Change in the emission intensity of chemosensor **2** after the addition of different metal ions (5 equiv.) in THF. (Bottom) Relative change in the emission intensity of chemosensor **2**.

Figure S5. (Top) Change in the emission intensity of chemosensor **3** after the addition of different metal ions (5 equiv.) in THF. (Bottom) Relative change in the emission intensity of chemosensor **3**.

Figure S6. Change in the emission intensity of **1** in THF on treatment with Cu(II) salts containing different anions.

Figure S7. Least-square fitting of fluorescent spectral changes of chemosensor **1** with Cu(II) ion using one site binding method.

Figure S8. Least-square fitting of fluorescent spectral changes of chemosensor **4** with Zn(II) ion using one site binding method.

Figure S9. (a) UV-visible titration profile of chemosensor **1** (50 μ M) in THF in the presence of increasing concentration of Cu(II) ion (50 to 100 μ M). Top inset: Mole ratio plot of **1** showing 1:1 stoichiometric change monitored at 335 nm, 310 nm and 260 nm.

Figure S10. Top panels: linear regression fitting curve for 1:1 binding between **1** and Cu(II) ion at 260 nm (a), 310 nm (b) and 335 nm (c). Bottom panels: Attempted linear regression fitting for 1:2 binding of chemosensor **1** with Cu(II) ion at 260 nm (a), 310 nm (b) and 335 nm (c).

Figure S11. Least-square fitting of absorption spectral changes of chemosensor **1** with Cu(II) ion at 260 nm, 310 nm and 335 nm using one site binding method.

Figure S12. UV-visible titration profile of chemosensor **4** (50 μ M) in THF in the presence of increasing concentration of Zn(II) ion (0 to 100 μ M). Inset: Mole ratio plot of **4** showing 1:1 stoichiometric change at 260, 310, and 335 nm.

Figure S13. Top panels: linear regression fitting curve for 1:1 binding between **4** and Zn(II) ion at 260 nm (a), 310 nm (b) and 335 nm (c). Bottom panels: attempted linear regression fitting for 1:2 binding of chemosensor **4** with Zn(II) ion at 260 nm (a), 310 nm (b) and 335 nm (c).

Figure S14. Least-square fitting of absorption spectral changes of chemosensor **4** with Zn(II) ion at 260 nm, 310 nm and 335 nm using one site binding method.

Figure S15. Comparative FTIR spectra of chemosensor **1** (black trace); copper complex **1-Cu** as synthesized after the reaction in THF (red trace); and the one crystallized from DMF (**1-Cu[#]**, blue trace).

Figure S16. (a) Full-range mass spectrum of Cu(II) complex **1-Cu** recorded in THF. (b) Relevant molecular ion peak with the simulated spectrum (bottom trace) of **1-Cu**. Simulated pattern was obtained from online chemical calculator (Institute of chemical sciences and engineering).

Figure S17. ESI-MS spectrum of **1-Cu[#]** recorded in MeOH.

Figure S18. ^1H NMR spectrum of **4-Zn** in DMSO-d_6 . * Represents the residual solvent peaks.

Figure S19. Comparative FTIR spectra of chemosensor **4** (black trace), Zn(II) complex **4-Zn** as synthesized after the reaction in THF (red trace) and the one crystallized from MeOH (**4-Zn**[#], blue trace).

Figure S20. (a) Full range mass spectrum of Zn(II) complex **4-Zn** recorded in THF. (b and c) Comparison of relevant molecular ion peaks with the simulated ones. Simulated patterns were obtained from the online chemical calculator (Institute of chemical sciences and engineering).

Figure S21. Thermal ellipsoidal representation of the crystal structure of **4-Zn**[#]; thermal ellipsoids are drawn at 30% level whereas all hydrogen atoms except those involved in hydrogen bonding have been omitted for clarity.

Figure S22. Change in the emission intensity of chemosensor **4** (0.1 mM) with the increasing concentration of Zn(II) ion (0-0.2 mM) in MeOH. Inset: Mole ratio plot exhibiting 1:1 stoichiometry between **4** and Zn(II) ion.

Figure S23. (above) ^1H NMR spectral titration of chemosensor **4** (1.0 mM) with increasing equivalents of Zn(II) ion (0-1.25 mM) in MeOH-d_4 . * Represents the residual solvent peaks. (below) Plot for the change in ^1H NMR chemical shifts of protons H_4 and H_2 with the increasing equivalents of Zn(II) ion.

Figure 24. (A) Bright field microscopic image of a crystal of chemosensor **4**. (B) Fluorescent image of **4** under 330 nm UV-light. (c) Change in the emission of **4** after treating with Zn(II) ion solution (1 mM) in water for 5 min.

Figure S25. Calculation of detection limit for chemosensor **1**.

Figure S26. Calculation of detection limit for chemosensor **4**.

Figure S27. Recyclability experiment of chemosensor **4** (black trace); after the addition of one equiv. of Zn(II) ion (red trace); followed by the addition of one equiv. of Na_2EDTA (green trace).

Figure S28. Solid-state diffuse reflectance absorption spectrum (blue trace) and THF solution absorption spectrum (black trace) of **1-Cu**.

Figure S29. Absorption spectra of **1-Cu**[#], in DMF (black traces) and diffuse reflectance (blue traces).

List of Tables

Table S1. Crystallographic data collection and structural refinement parameters for chemosensor **1**, **1-Cu[#]** and **4-Zn[#]**.

Table S2. Selected bond distances (Å) and bond angles (°) for **1-Cu[#]** and **4-Zn[#]**.

Table S3. A comparative table displaying the chemosensing abilities of assorted receptors reported in the literature along with chemosensors **1** and **4** (Present work).

1. Experimental Section

Synthesis. All reagents and chemicals of analytical grade were commercially available and used as received without further purification unless otherwise stated. Solvents were purified according to the standard literature procedure.¹ Chemosensor **1** was synthesized as per our earlier report.²

2. Synthesis of Chemosensors.

Chemosensor 2. Pyridine-2,6-dicarboxylic acid (1.0 g, 0.0059 mol) and 2-aminobenzimidazole (1.59g, 0.0119 mol) were taken in 25 ml pyridine and refluxed with stirring for 30 min at 120 °C. Triphenylphosphite (3.87 g, 0.015 mol) was added drop-wise to the reaction mixture and the reaction mixture was further stirred at 100 °C for additional 6 h. The reaction mixture was cooled to room temperature and poured to the ice-cold water. This resulted in the precipitation of a pale yellow product, which was filtered, washed with water and air dried. The crude product was recrystallized from THF. Yield 2.10 g (88 %). FT-IR spectrum (Zn–Se ATR, cm⁻¹): 3376 and 3235(N-H), 1686 (C=O) cm⁻¹. ¹H NMR spectrum (400MHz, d₆-DMSO): δ = 13.10 (broad, CONH), 8.516 (d, *J*=8.0Hz, 2H), 8.392 (t, *J*=8.04Hz, 1H), 7.560 (q, *J*=3.64 Hz, 4H), 7.188 (q, *J*=2.92Hz, 4H), 3.152 (s, 2H {-NH}). ¹³C NMR spectrum (DMSO-*d*₆, 100 MHz): δ = 165.39 (C₅), 162.10 (C₄), 148.50 (C₃), 146.19(C₂), 136.31(C₁), 128.86 (C₁₁), 126.71 (C₆), 125.54 (C₁₀ + C₇), 120.81 (C₈ + C₉).

Chemosensor 3. Pyridine-2,6-dicarboxylic acid (10g, 0.059 mol) was added as a solid in one portion to a suspension of a 1:1 mixture of 2-aminobenzothiazole (8.98g, 0.059 mol) and *para*-anisidine (7.39g, 0.059 mol) in pyridine (40 mL). The mixture was stirred at 80 °C for 40 min. Triphenylphosphite (40.8g, 0.013 mol) was added drop-wise over 10 min, after which the temperature of the mixture was increased to 100 °C. The reaction mixture was stirred for 4 h at 100 °C. The reaction mixture was allowed to attain room temperature followed by pouring to ice-cold water. This resulted in the precipitation of a white product, which was filtered and washed with aqueous methanol (5%, v/v) and air dried. The crude product thus obtained was purified by the column chromatography on silica gel using chloroform/methanol mixture (5/1, v/v) as the eluent. Yield 10.04 g, (41.0 %). Anal. Calc. for C₂₁H₁₆N₄O₃S: C, 62.36; H, 3.99; N, 13.85; S, 7.93. Found: C, 61.86; H, 3.72; N, 14.12; S, 8.10. Mass spectrum (ESI⁺, MeOH, *m/z*): calc. 404.0943 for **3**; found 405.1016 for **3** + H⁺; found 427.0831 for **3** + Na⁺. FTIR spectrum(Zn-Se, cm⁻¹, selected peaks): 3337, 3280 (NH), 1656, 1600 (C=O). ¹H NMR spectrum (400 MHz, CDCl₃): δ 11.79 (s, 1H (broad, CONH)), 9.90 (s, 1H (CONH)), 8.53 (d, *J* = 7.5 Hz, 1H), 8.44 (d, *J* = 7.7 Hz, 1H), 8.12 (t, *J* = 7.7 Hz, 1H), 7.84 (d, *J* = 5.3 Hz, 1H), 7.75 (t, *J* = 6.8 Hz, 2H), 7.45 (dd, 1H), 7.34 (t, *J* = 7.3 Hz, 2H), 6.88 (d, *J* = 6.4 Hz, 2H), 3.80 (s, 3H). ¹³C NMR spectrum (DMSO-*d*₆, 100 MHz): δ = 162.49 (C₇), 161.40 (C₁₄), 159.20 (C₆), 158.12 (C₁₈), 150.14 (C₁₃), 148.20 (C₁), 146.39(C₅), 139.85(C₃), 134.43(C₈), 132.15 (C₁₅), 126.26 (C₁₁), 125.80 (C₂), 124.14 (C₄), 123.52 (C₁₆₊₂₀), 123.11 (C₁₀), 122.21 (C₉), 120.01 (C₁₂), 115.13 (C₁₇₊₁₉), 58.21 (C_{OMe}).

Chemosensor 4. To a solution of pyridine-2-carboxylic acid (1.0 g, 0.0059 mol) in pyridine (30 mL) was added 2-aminobenzothiazole (0.89g, 0.0059 mol) and triphenylphosphite (3.87 g, 0.015 mol) while stirring. The resulting mixture was further stirring for 6h at 110 °C. Hot reaction mixture was cooled to ambient temperature and poured into ice cold water resulting in immediate precipitation. The white solid thus separated was filtered and washed thoroughly with cold water. Resulted compound was air dried and washed with cold methanol (10 ml). Yield 1.80 g, (86 %). Anal. Calc. for C₁₃H₉N₃OS: C, 61.16; H, 3.55; N, 16.46; S, 12.56. Found: C, 61.36; H, 3.15; N, 15.96; S, 13.01. MS spectrum (ESI⁺, MeOH, *m/z*): calc. 255.0466 for **4**; found 256.0543 for **4** + H⁺; found 511.1049 for (**4**)₂ + H⁺. FTIR spectrum(Zn-Se, cm⁻¹, selected peaks): 3370 (NH), 1690 (C=O). ¹H NMR spectrum (400 MHz, DMSO-D₆) δ 12.21 (s, 1H), 8.76 (d, *J* = 4.6 Hz, 1H), 8.19 (d, *J* = 7.6 Hz, 1H), 8.09 (t, *J* = 7.8 Hz, 1H), 8.02 (d, *J* = 7.9 Hz, 1H), 7.79 (d, *J* = 8.1 Hz, 1H), 7.72 (dd, *J* = 7.5, 4.5 Hz, 1H), 7.45 (t, *J* = 7.6 Hz, 1H), 7.33 (t, *J* = 7.6 Hz, 1H). ¹³C NMR

spectrum (DMSO- D_6), δ = 164.30 (C_7), 157.91 (C_6), 149.62 (C_{13}), 148.33 (C_5), 138.88 (C_1), 132.25 (C_3), 128.52 (C_8), 126.85 (C_2), 124.47 (C_{11}), 123.76 (C_{10}), 122.42 (C_4+C_9), 121.37 (C_{12}).

3. Synthesis of Metal Complexes

[Cu(1)(H₂O)₂](ClO₄)₂ (1-Cu). To a THF (10 ml) solution of **1** (0.1g, 0.232 mmol)[Cu(H₂O)₆](ClO₄)₂ (0.08 g, 0.232 mmol) dissolved in THF (10 ml) was added drop-wise while stirring. The resulting green solution was finally stirred for 1 h. The reaction mixture was passed through a pad of cellite in a medium porosity frit and the filtrate was left for evaporation. Green crystalline material was appeared after 12h. This product was filtered, washed with diethyl ether and dried. Yield: 0.14 g (85%). FTIR spectrum (Zn-Se, cm^{-1} , selected peaks): 3285 (NH), 1660 (C=O). Molar conductivity (DMF ~ 1 mM solution, 298 K): $\Lambda_M = 155 \Omega^{-1} cm^2 mol^{-1}$ (the range for 1:2 electrolyte in DMF is 130–170). Anal. Calc. for **1-Cu** (C₂₁H₁₉N₅O₁₂S₂Cl₂Cu): C, 34.46; H, 2.62; N, 9.57; S, 8.76. Found: C, 34.81; H, 2.91; N, 9.37; S, 8.37. MS spectrum (ESI⁺, THF, m/z): calc. 727.8988 for **1-Cu**; found 729.1520 for **1-Cu** +H⁺; found 592.9304 for **1-Cu** – ClO₄.

[Cu(1-2H⁺)(H₂O)](1-Cu[#]). Complex **1-Cu** (0.1g) was dissolved in DMF (5ml) and vapor of diethyl ether were diffused at room temperature. Dark green crystals suitable for X-ray diffraction studies were isolated within 24 h. Yield: 0.052 g (74%). FTIR spectrum (Zn-Se, cm^{-1} , selected peaks): 1637 (C=O). Anal. Calc. for **1-Cu[#]** (C₂₁H₁₃N₅O₃S₂Cu): C, 49.36; H, 2.56; N, 13.70; S, 12.55. Found: C, 48.91; H, 2.91; N, 13.57; S, 12.37. MS spectrum (ESI⁺, MeOH or MeCN, m/z): calc. 527.9861 for **1-Cu[#]** + H₂O; found 528.9484 for **1-Cu[#]** + H₂O + H⁺.

[Zn(4)(ClO₄)₂] (4-Zn). The complex **4-Zn** was synthesized in a similar manner as mentioned for **1-Cu**, however, using **4** (0.1 g, 0.392 mmol) and [Zn(H₂O)₆](ClO₄)₂ (0.143 g, 0.0023 mol). Yield: 0.186 g (92 %). FTIR spectrum (Zn-Se, cm^{-1} , selected peaks): 3560 (broad, -NH), 1510 (C=O). Molar conductivity (DMF ~ 1 mM solution, 298 K): $\Lambda_M = 165 \Omega^{-1} cm^2 mol^{-1}$ (the range for 1:2 electrolyte in DMF is 130–170). Anal. Calc. for **4-Zn** (C₁₃H₉N₃O₉SCl₂Zn): Calc.: C, 30.05; H, 1.75; N, 8.09; S, 6.17. Found: C, 29.60; H, 1.92; N, 8.24; S, 5.92. MS spectrum (ESI⁺, THF, m/z): calc. 417.9243; found 417.9279 for [Zn(**4**)(ClO₄)₂]⁺. ¹H NMR spectrum (400 MHz,

d6-DMSO): δ = 13.39 (s, -NH), 8.44 (d, J = 8.1 Hz, 2H), 8.38(dd, J = 7.2–8.2 Hz, 1H), 7.66 (d, J = 3.7 Hz, 2H), 7.40 (d, J = 3.7 Hz, 2H).

[Zn(4)₂(ClO₄)₂] (4-Zn[#]). Complex 4-Zn (0.1 g) was dissolved in MeOH (5ml) followed by the vapor diffusion of diethyl ether at room temperature. Pale yellow crystalline product was isolated within 3 d. Yield: 0.025 g (66%). FTIR spectrum (Zn-Se, cm⁻¹, selected peaks): 3496 (broad, -NH), 1502 (C=O) cm⁻¹. Molar conductivity (DMF ~ 1 mM solution, 298 K): Λ_M = 158 $\Omega^{-1}\text{cm}^2\text{mol}^{-1}$ (the range for 1:2 electrolyte in DMF is 130–170). Anal. Calc. for 4-Zn[#](C₂₆H₁₈N₆O₁₀S₂Cl₂Zn): Calc.: C, 40.30; H, 2.34; N, 10.85; S, 8.28. Found: C, 40.60; H, 2.16; N, 10.64; S, 8.02. MS spectrum (ESI⁺, THF or MeOH, m/z): calc 573.0146; found 573.0149 for 4-Zn[#]–H]⁺.

4. Physical Measurements. The conductivity measurements were carried out with a digital conductivity bridge from the Popular Traders, India (model number: PT 825). The elemental analysis data were obtained with an Elementar Analysen Systeme GmbH Vario EL-III instrument. The NMR spectral measurements were carried out with a Jeol 400 MHz instrument. The Zn–Se ATR FTIR spectra were recorded with a Perkin-Elmer Spectrum-Two spectrometer. The absorption spectra were recorded with a Perkin-Elmer Lambda 25 spectrophotometer. Fluorescence studies were performed with a Carry Eclipse fluorescence spectrometer.

5. Crystallography. The intensity data for **1**, **1-Cu[#]** and **4-Zn[#]** were collected with Oxford XCalibur CCD diffractometer using graphite-monochromated Mo-K α radiation (λ = 0.71073 Å).³ The frames were collected at room temperature. A multi-scan absorption correction was applied using CrysAlis-PRO.³ The structures were solved by the direct methods using SIR-92⁴ and refined by the full-matrix least squares refinement techniques on F^2 using SHELXL97.⁵ The hydrogen atoms were placed at the calculated positions and included in the last cycles of the refinement. All calculations were done using the WinGX software package.⁶ For **4-Zn[#]**, both ClO₄⁻ ions were refined with half occupancy. This was due to the presence of zinc metal on the mirror plane. Details of the crystallographic data collection and structural solution parameter are provided in Table S1. In addition, Table S2 contained the selected bond distances and bond angles for **1-Cu[#]** and **4-Zn[#]**.

6. Fabrication of films and strips.

6. 1. Fabrication of polystyrene films. Chemosensor **1** dissolved in THF (1 ml) was added to styrene (1 ml) containing α,α' -azoisobutyronitrile (AIBN; 1 mg). The resulting clear solution was heated on water bath at 80 °C for 1 h. Finally, a few drops of hot solution were poured over cover-glass slide and allowed to attain room temperature. In case of chemosensor **4**, solution was made by directly adding **4** to styrene (1 ml) containing AIBN and heating to 80°C on water bath.

6.2. Fabrication of filter paper test strips. In as typical experiment, a strip of Whatman filter paper was dipped in a solution of chemosensor **1** or **4** in THF and was air-dried. Test strips coated with either chemosensor **1** or **4** were dipped directly into the Cu(II) or Zn(II) solution in THF for a couple of seconds. Such strips were then investigated using the table top Uv-vis. lamp.

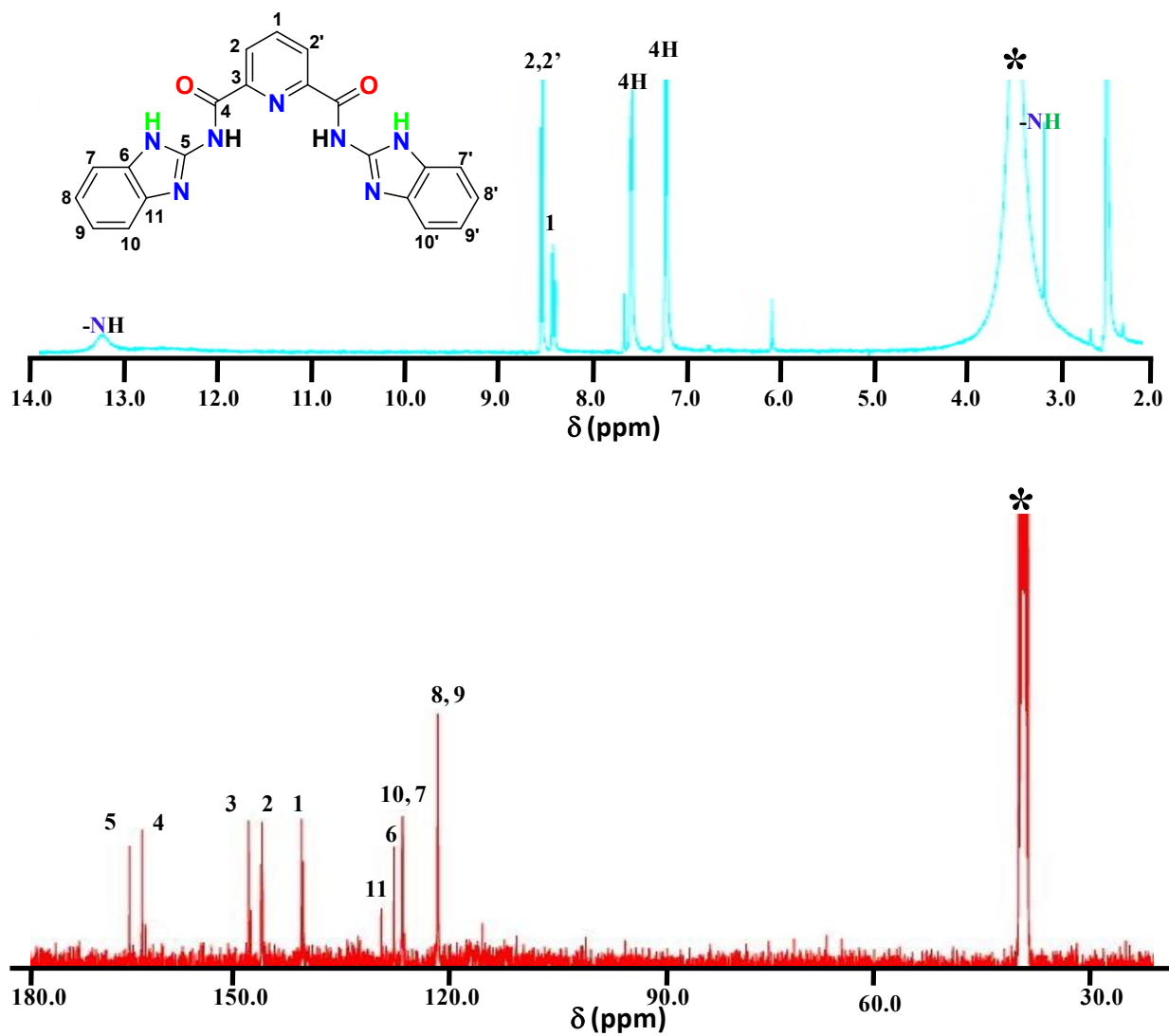


Figure S1. ^1H (top) and ^{13}C NMR (bottom) spectra of chemosensor **2** in DMSO-d_6 . * Represents the residual solvent peak.

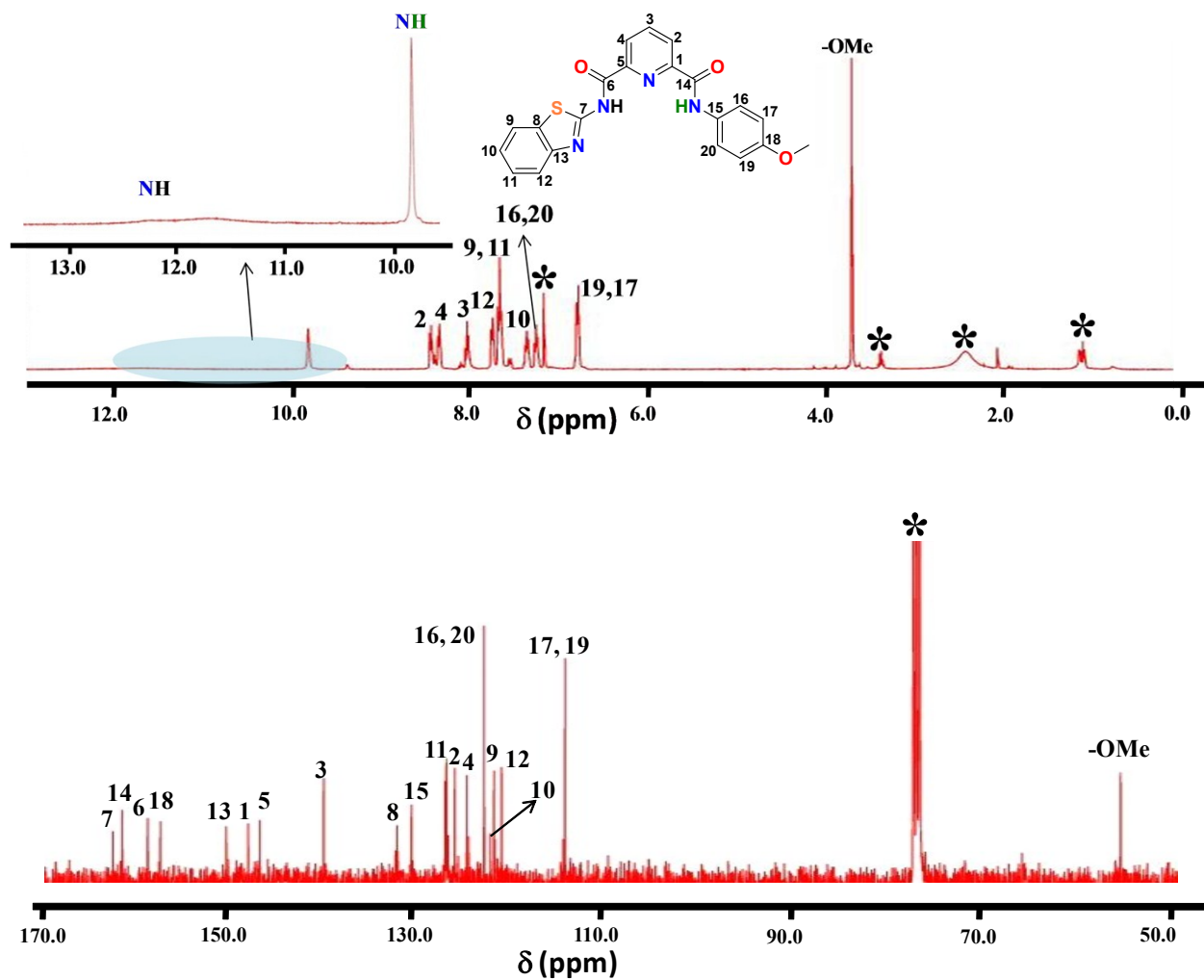


Figure S2. ^1H (top) and ^{13}C NMR (bottom) spectra of chemosensor **3** in DMSO-d_6 . * Represents the residual solvent peak(s).

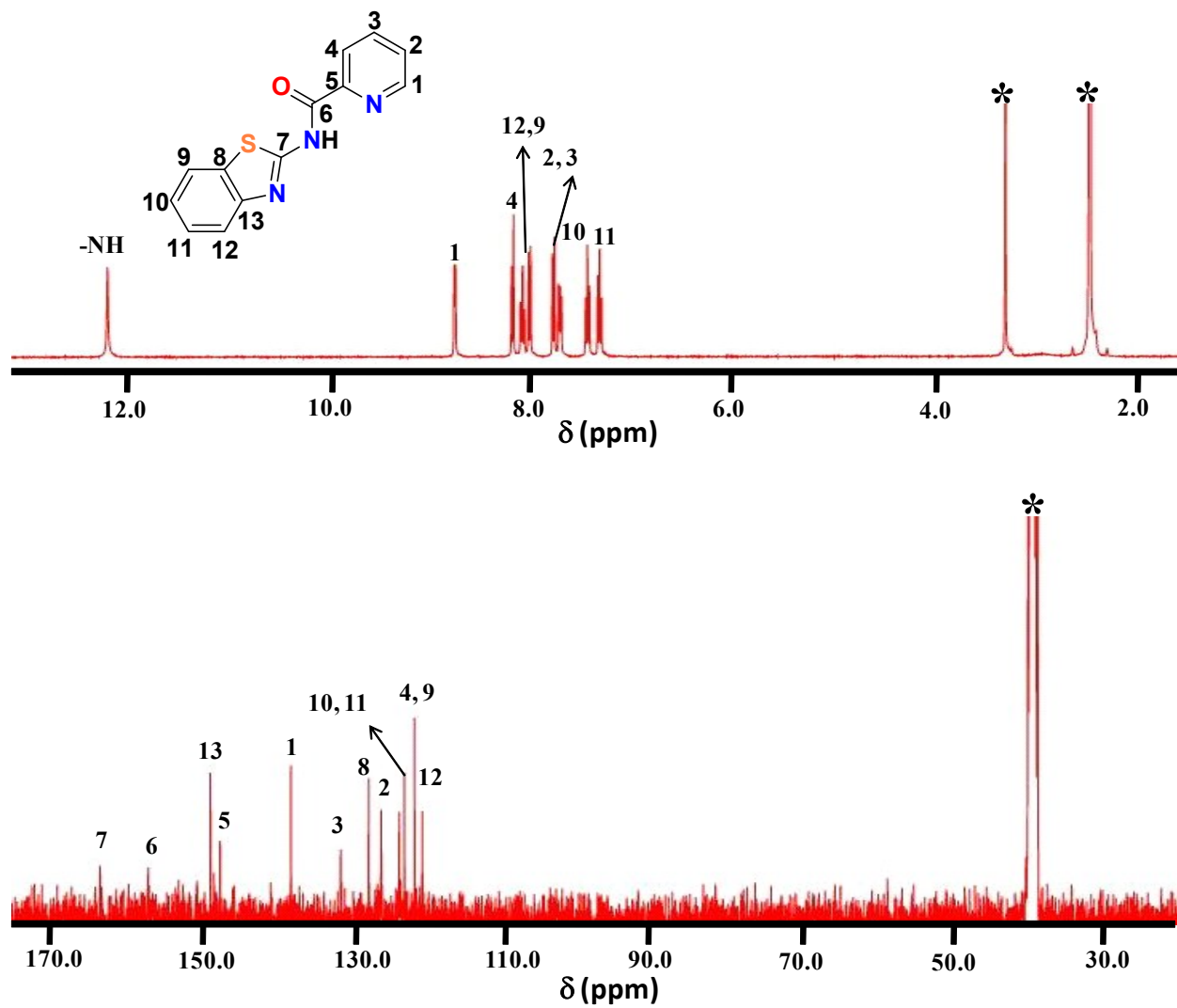


Figure S3. ¹H (top) and ¹³C NMR (bottom) spectra of chemosensor4 in DMSO-d₆. * Represents the residual solvent peak(s).

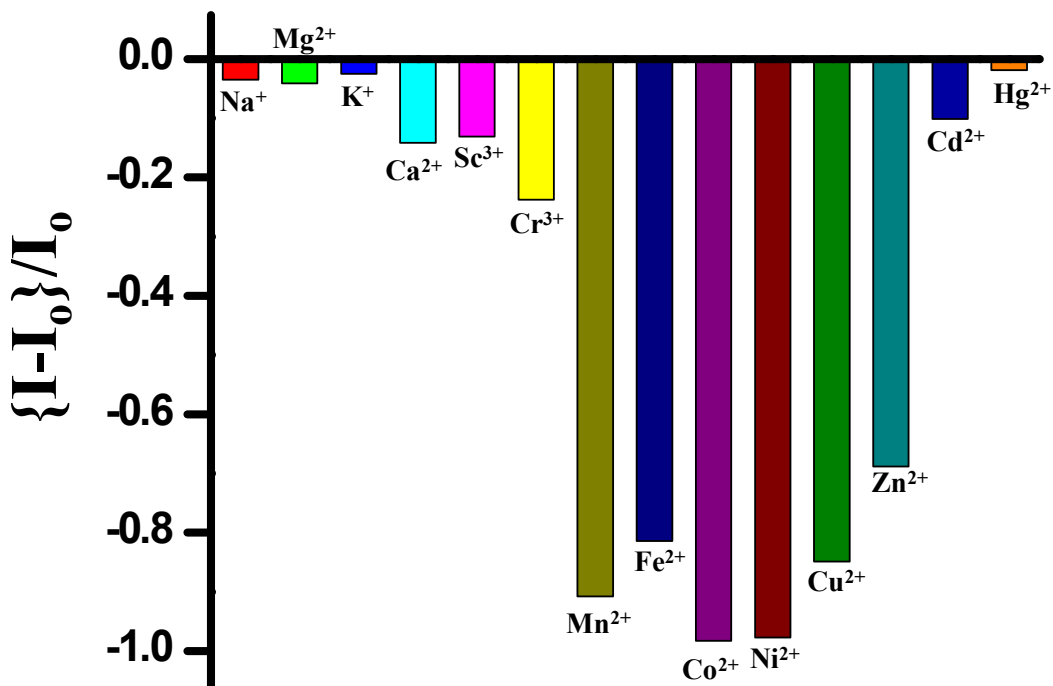
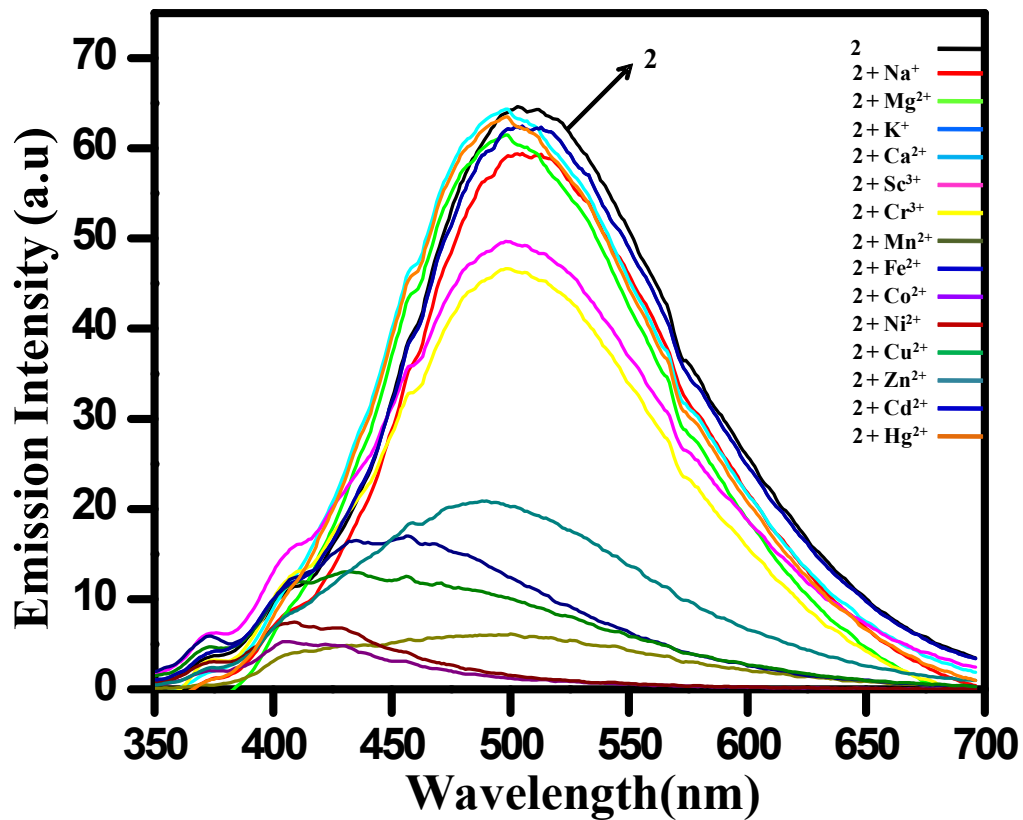


Figure S4. (Top) Change in the emission intensity of chemosensor **2** after the addition of different metal ions (5 equiv.) in THF. (Bottom) Relative change in the emission intensity of chemosensor **2**.

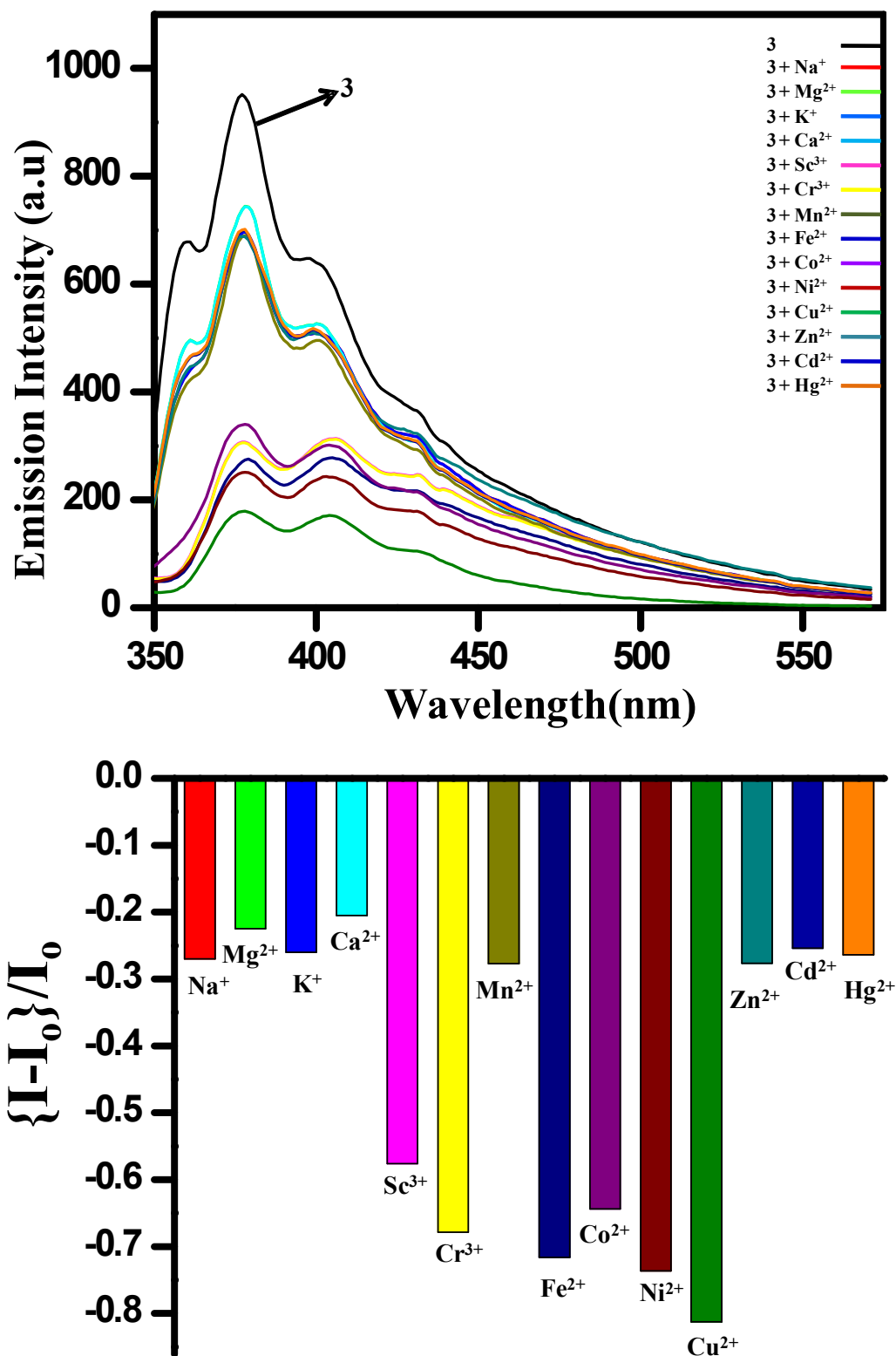


Figure S5. (Top) Change in the emission intensity of chemosensor **3** after the addition of different metal ions (5 equiv.) in THF. (Bottom) Relative change in the emission intensity of chemosensor **3**.

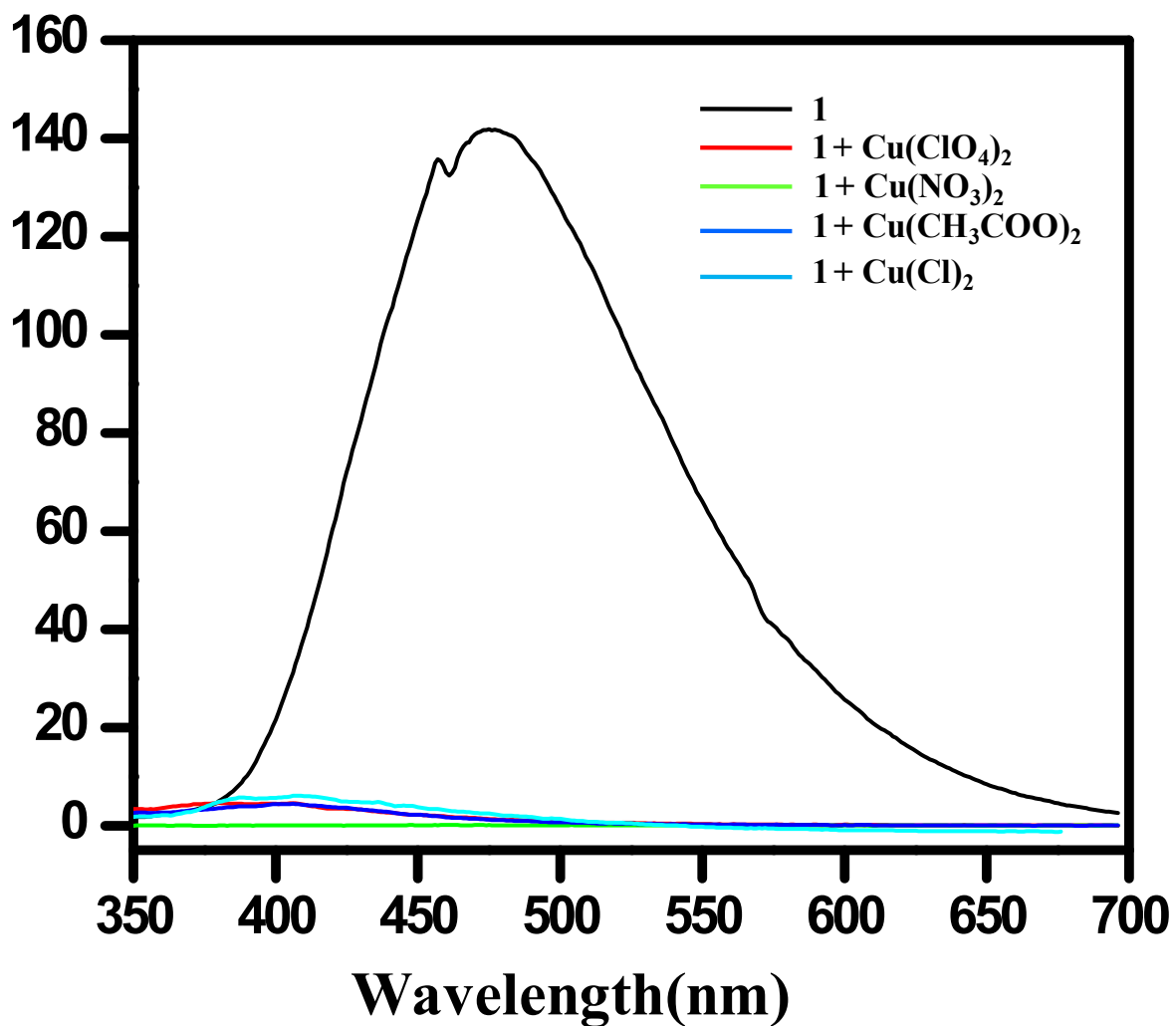


Figure S6. Change in the emission intensity of **1** in THF on treatment with Cu(II) salts containing different anions.

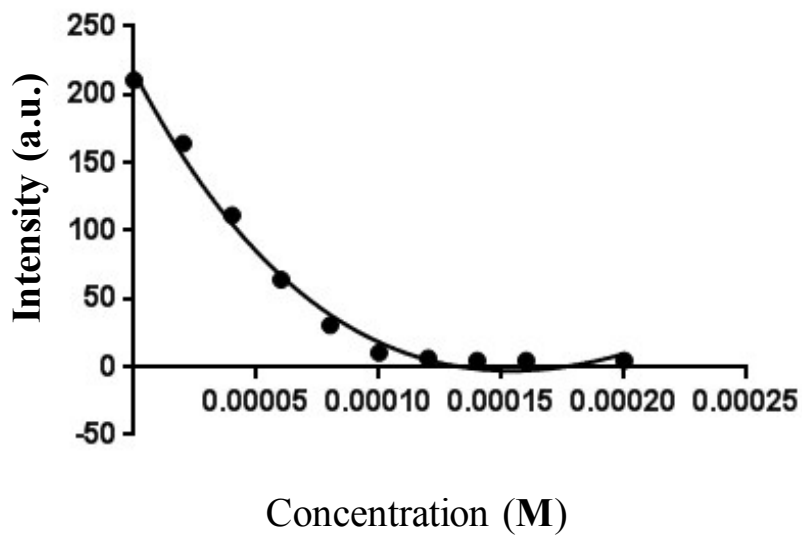


Figure S7. Least-square fitting of fluorescent spectral changes of chemosensor **1** with Cu(II) ion using one site binding method.

Fitting method	Conc. Cu ²⁺	Conc. Ligand	Mole Ratio
One site – total binding	0.083	0.1	0.84

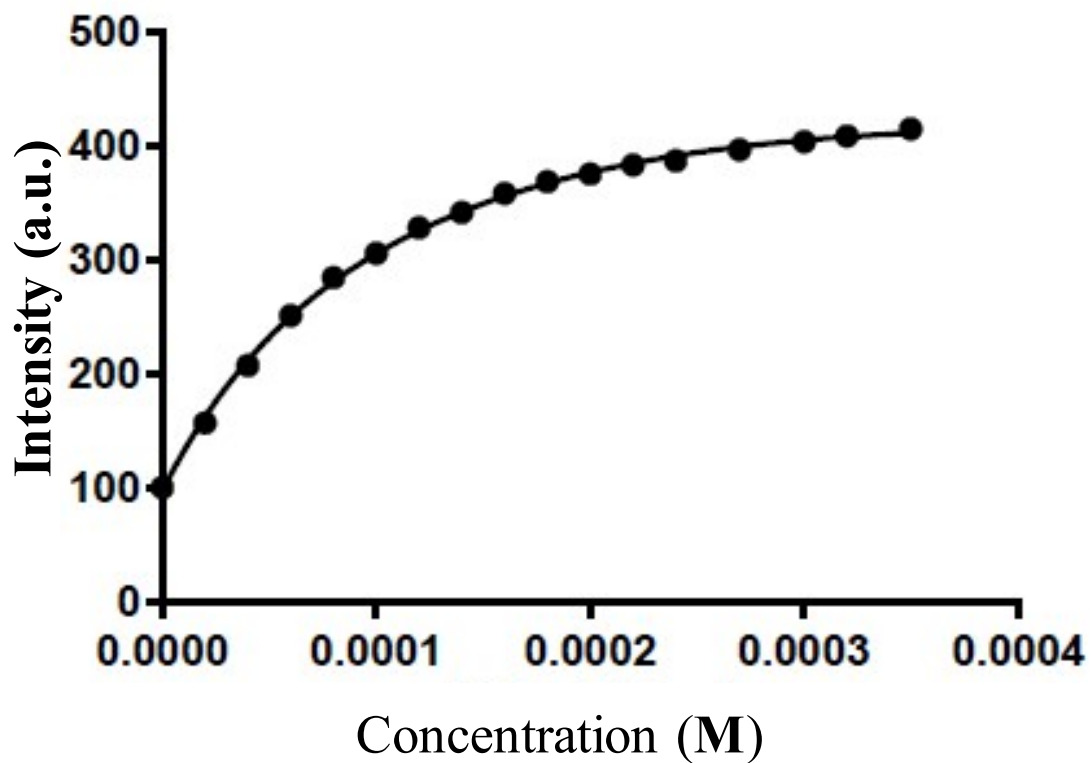


Figure S8. Least-square fitting of fluorescent spectral changes of chemosensor **4** with Zn(II) ion using one site binding method.

Fitting method	Conc. Zn ²⁺	Conc. Ligand	Mole Ratio
One site – total binding	0.09862	0.1	0.99

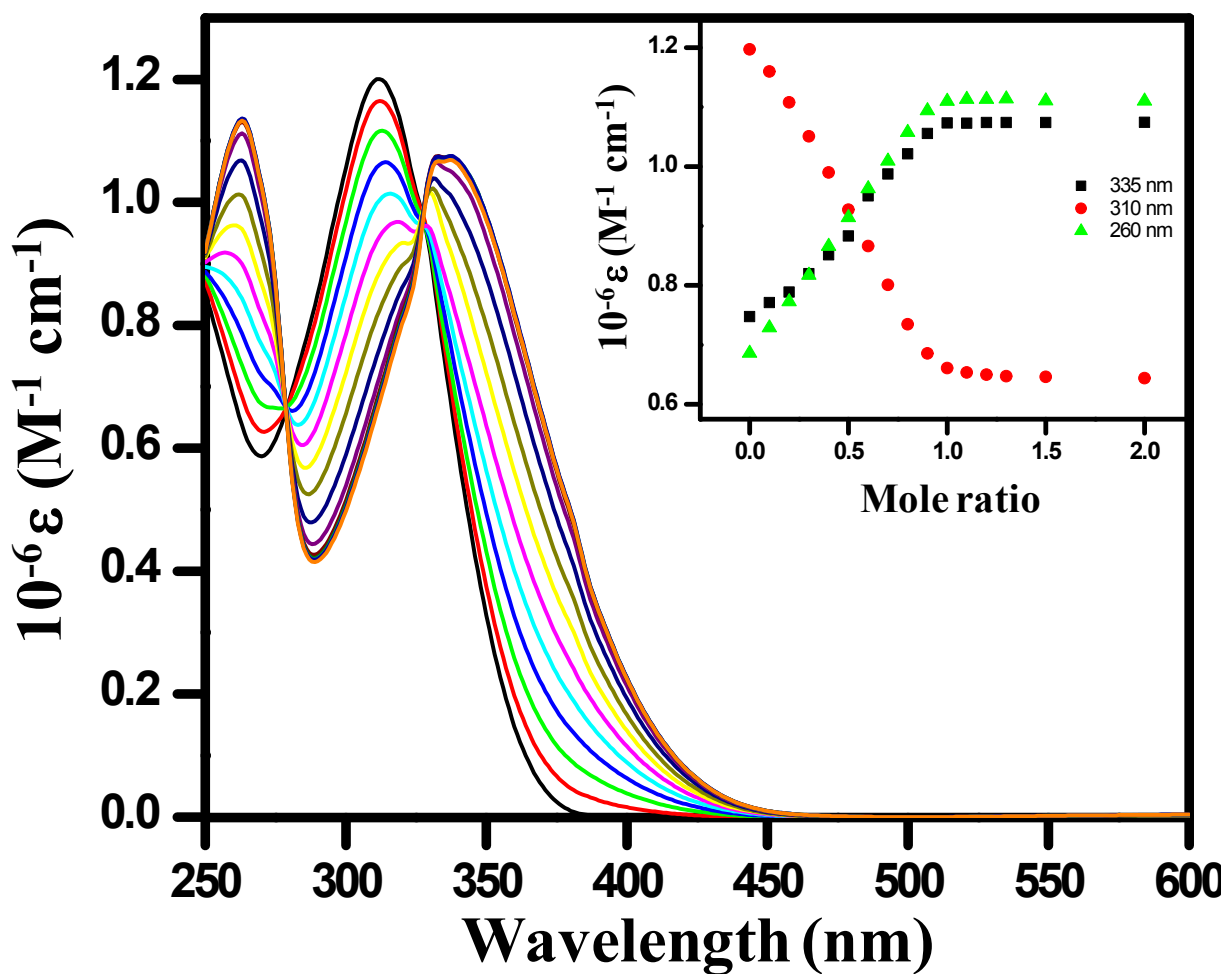


Figure S9. (a) UV-visible titration profile of chemosensor **1** (50 μM) in THF in the presence of increasing concentration of Cu(II) ion (50 to 100 μM). Top inset: Mole ratio plot of **1** showing 1:1 stoichiometric change monitored at 335 nm, 310 nm and 260 nm.

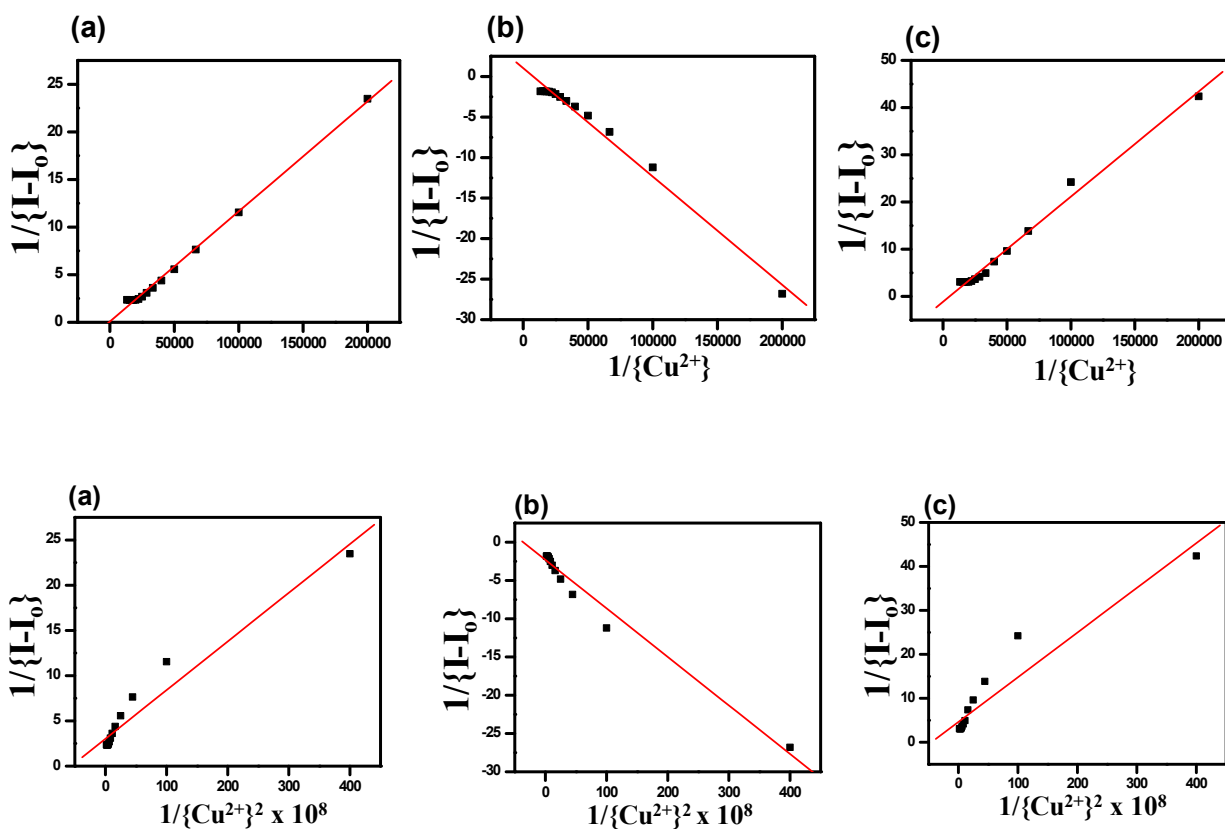


Figure S10. Top panels: linear regression fitting curve for 1:1 binding between **1** and Cu(II) ion at 260 nm (a), 310 nm (b) and 335 nm (c). Bottom panels: Attempted linear regression fitting for 1:2 binding of chemosensor **1** with Cu(II) ion at 260 nm (a), 310 nm (b) and 335 nm (c).

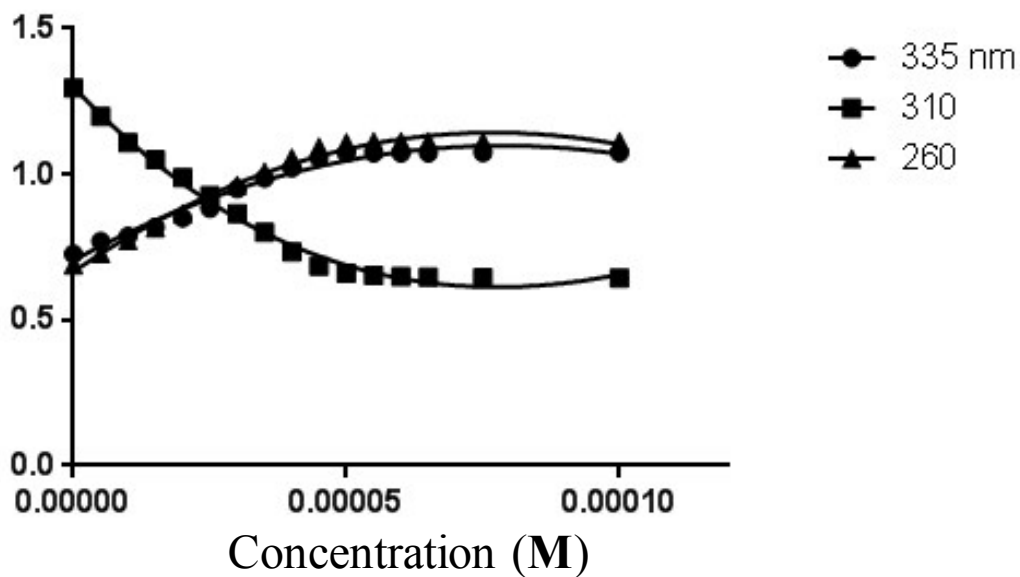


Figure S11. Least-square fitting of absorption spectral changes of chemosensor 1 with Cu(II) ion at 260 nm, 310 nm and 335 nm using one site binding method.

Fitting method	Wavelength (nm)	Conc. Cu ²⁺	Conc. Ligand	Mole Ratio
One site – Total binding	310	0.000052 M	0.00005	1.04
One site – Total binding	260	0.000064 M	0.00005	1.28
One site – Total binding	335	0.000065 M	0.00005	1.29

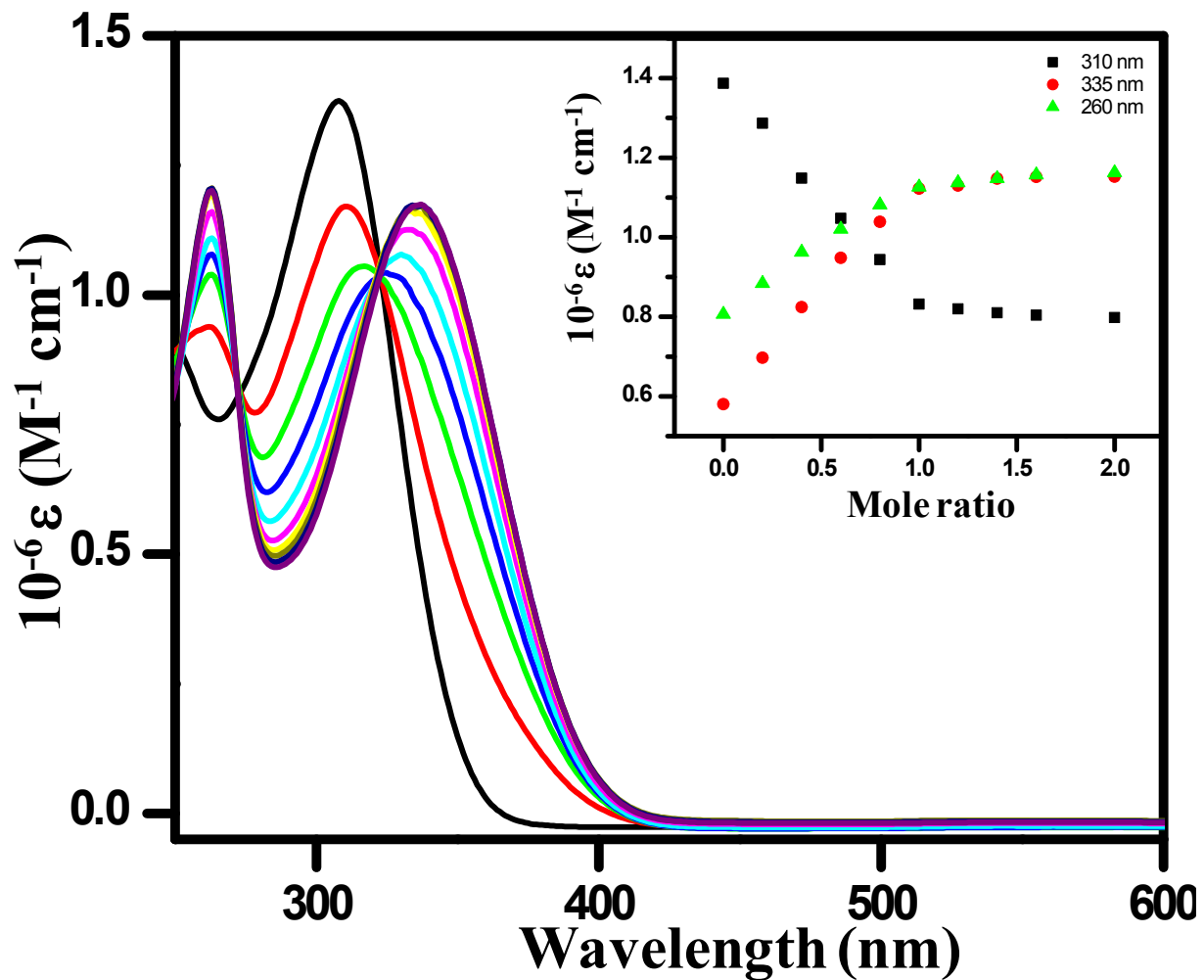


Figure S12. UV-visible titration profile of chemosensor 4 (50 μ M) in THF in the presence of increasing concentration of Zn(II) ion (0 to 100 μ M). Inset: Mole ratio plot of 4 showing 1:1 stoichiometric change at 260, 310, and 335 nm.

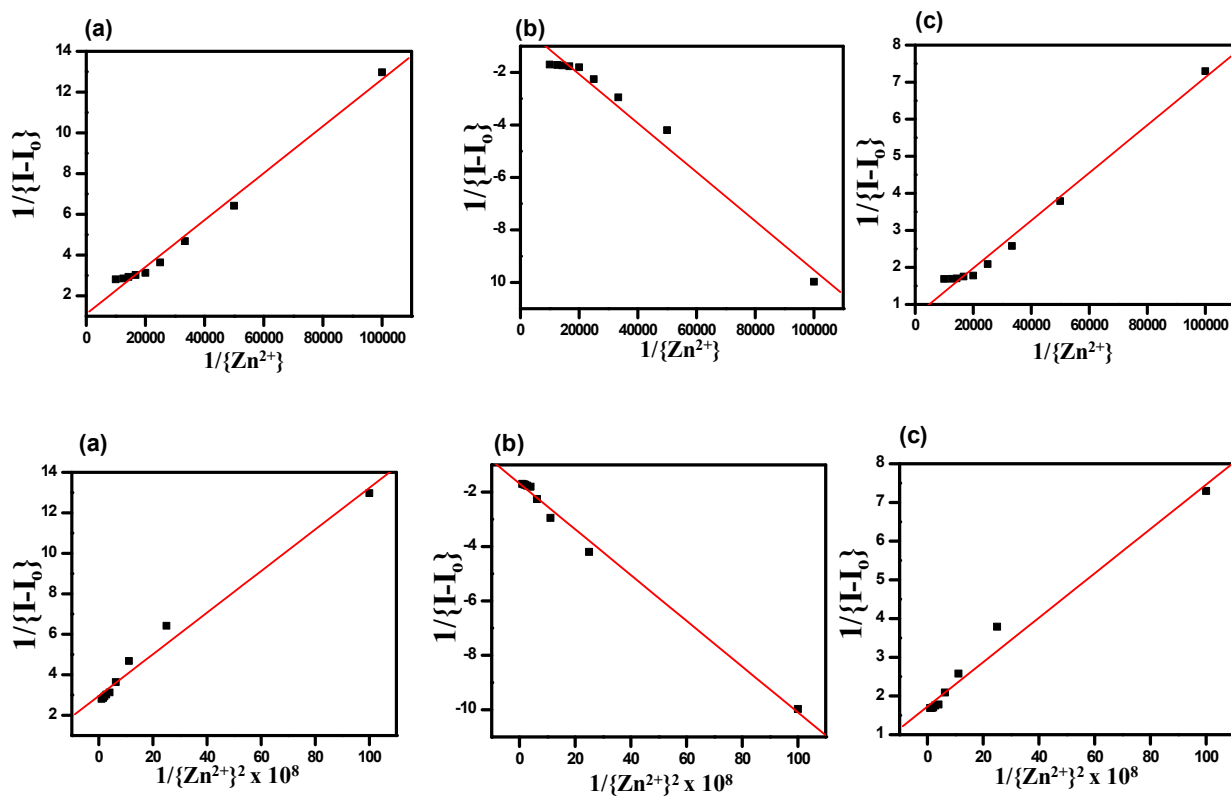


Figure S13. Top panels: linear regression fitting curve for 1:1 binding between **4** and Zn(II) ion at 260 nm (a), 310 nm (b) and 335 nm (c). Bottom panels: attempted linear regression fitting for 1:2 binding of chemosensor **4** with Zn(II) ion at 260 nm (a), 310 nm (b) and 335 nm (c).

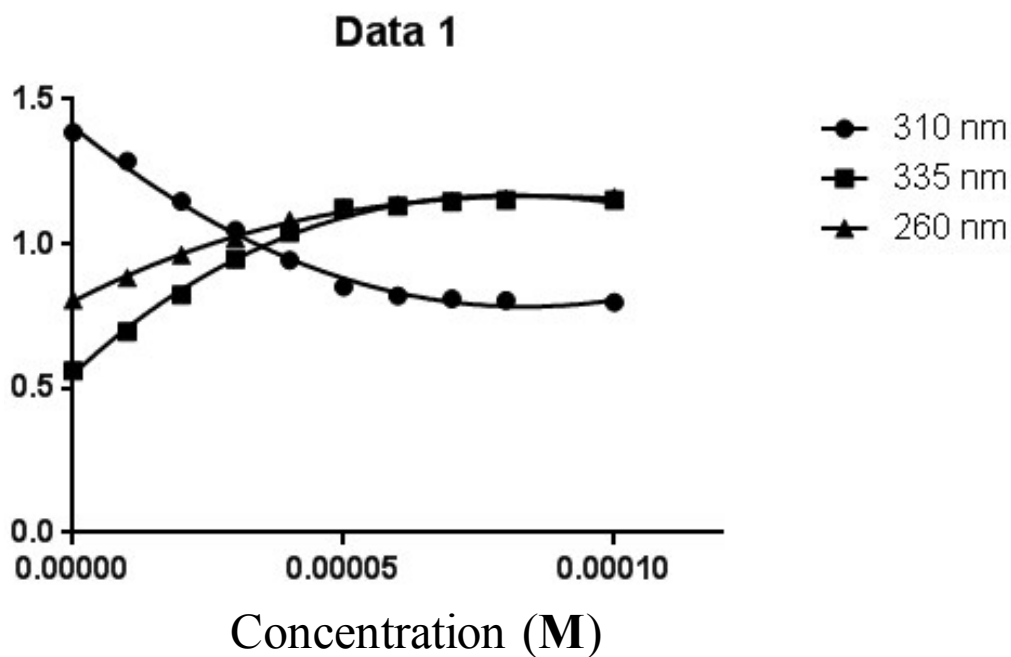


Figure S14. Least-square fitting of absorption spectral changes of chemosensor **4** with Zn(II) ion at 260 nm, 310 nm and 335 nm using one site binding method.

Fitting method	Wavelength (nm)	Conc. Zn ²⁺	Conc. Ligand	Mole Ratio
One site – Total binding	310	0.0000399 M	0.00005	0.80
One site – Total binding	260	0.0000571 M	0.00005	1.14
One site – Total binding	335	0.00005708 M	0.00005	1.14

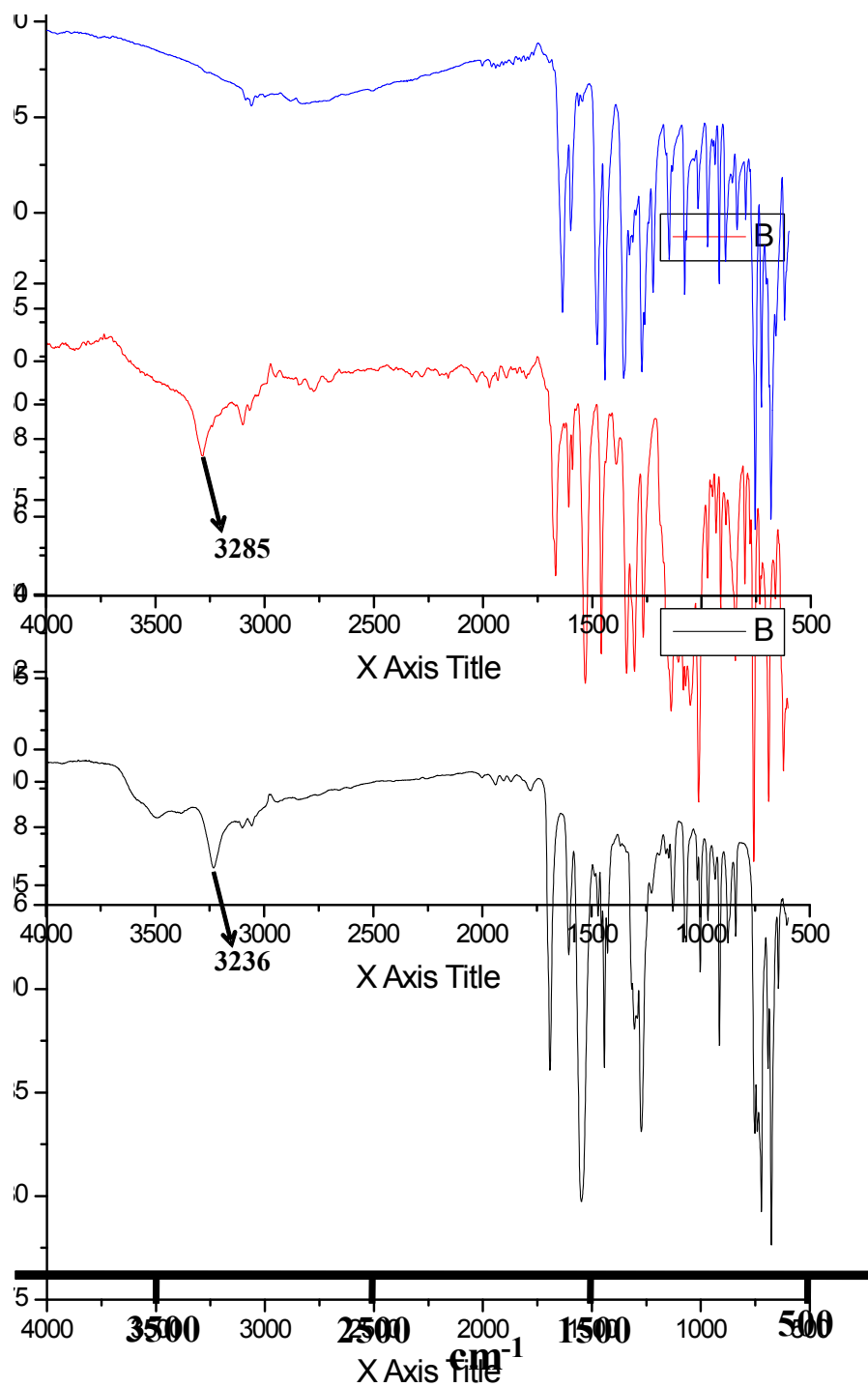


Figure S15. Comparative FTIR spectra of chemosensor **1** (black trace); copper complex **1-Cu** as synthesized after the reaction in THF (red trace); and the one crystallized from DMF (**1-Cu[#]**, blue trace).

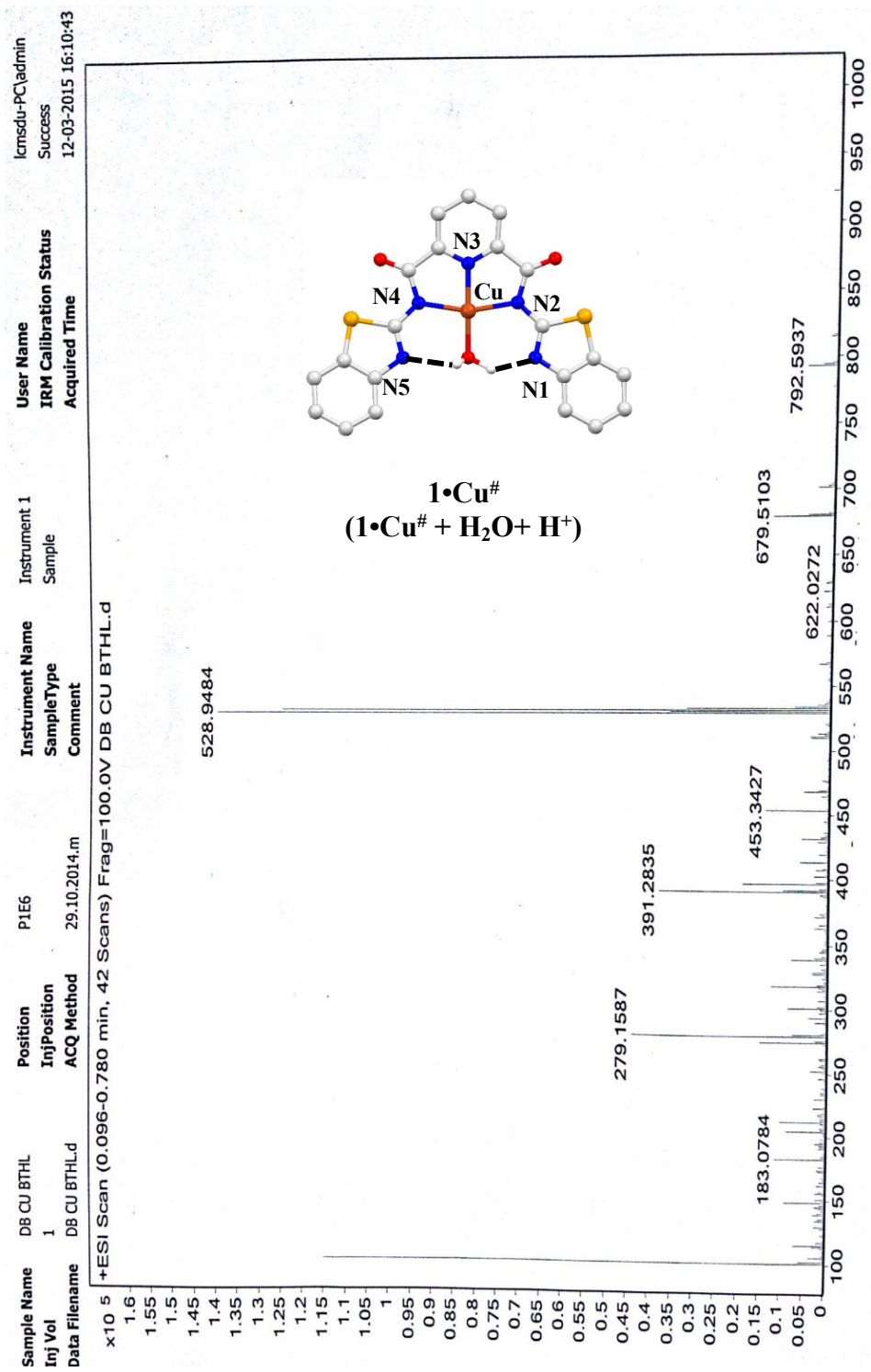


Figure S17. ESI-MS spectrum of **1-Cu[#]** recorded in MeOH.

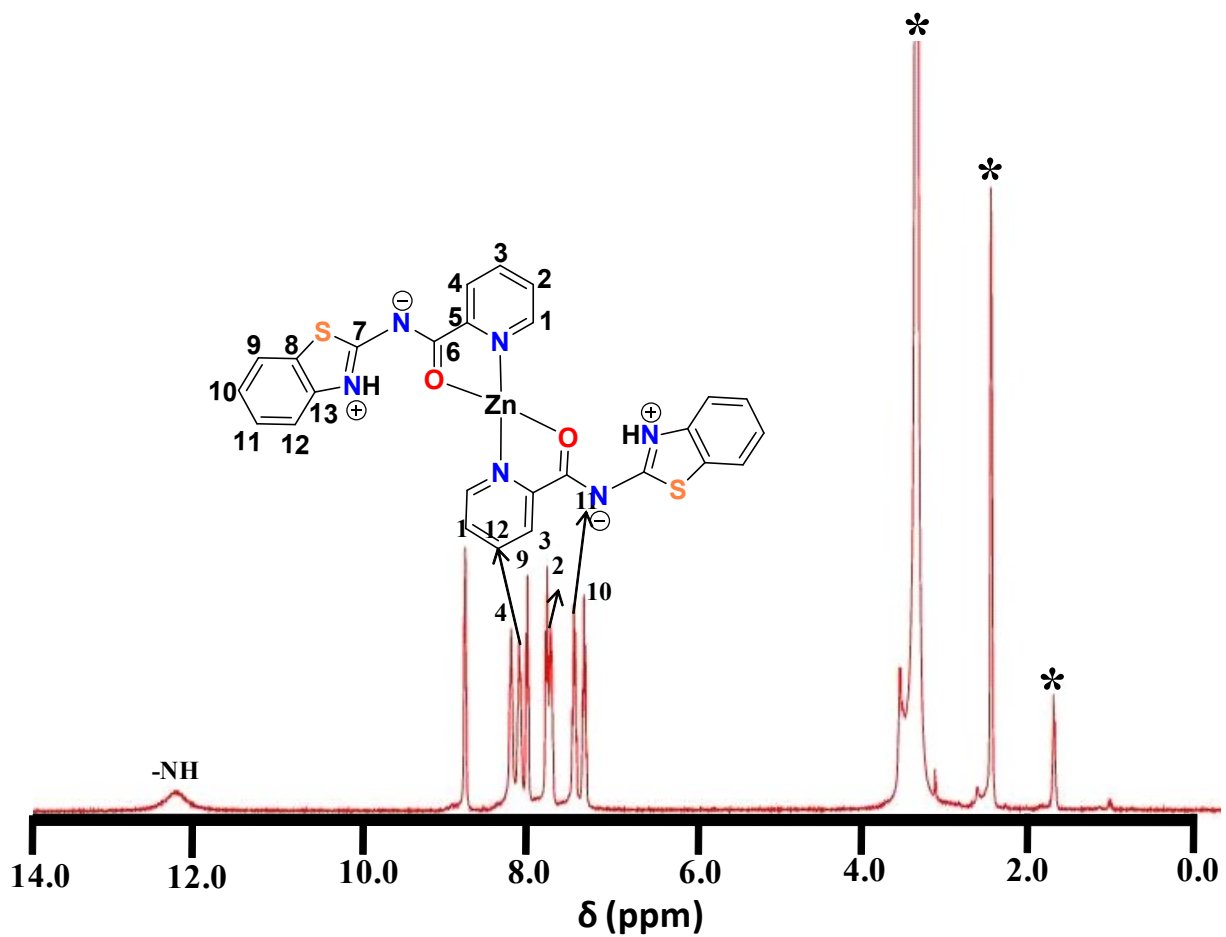


Figure S18. ¹H NMR spectrum of 4-Znin in DMSO-d₆. * Represents the residual solvent peaks.

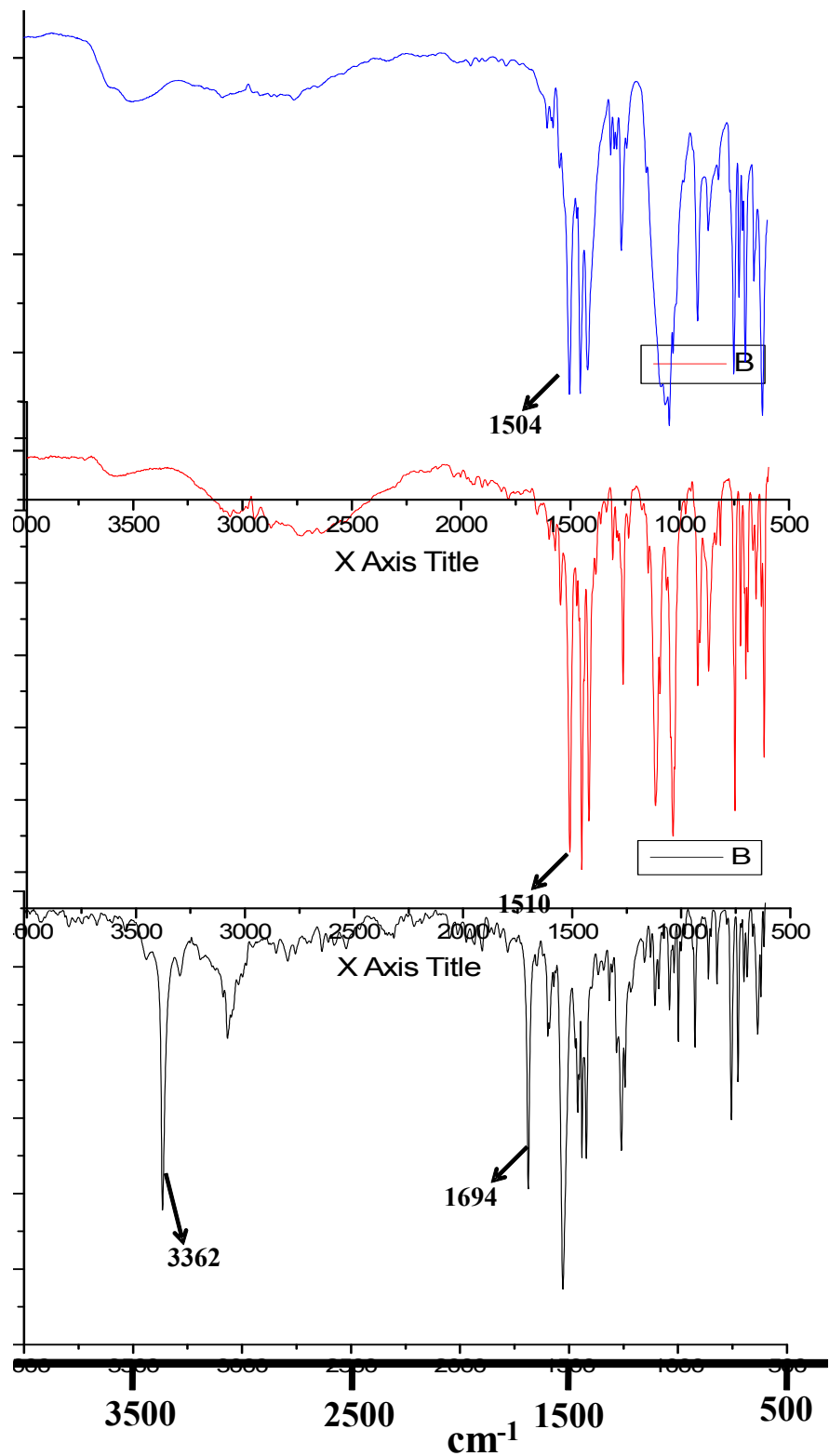


Figure S19. Comparative FTIR spectra of chemosensor **4**(black trace), Zn(II) complex **4-Zn** synthesized after the reaction in THF (red trace) and the one crystallized from MeOH (**4-Zn[#]**, blue trace).

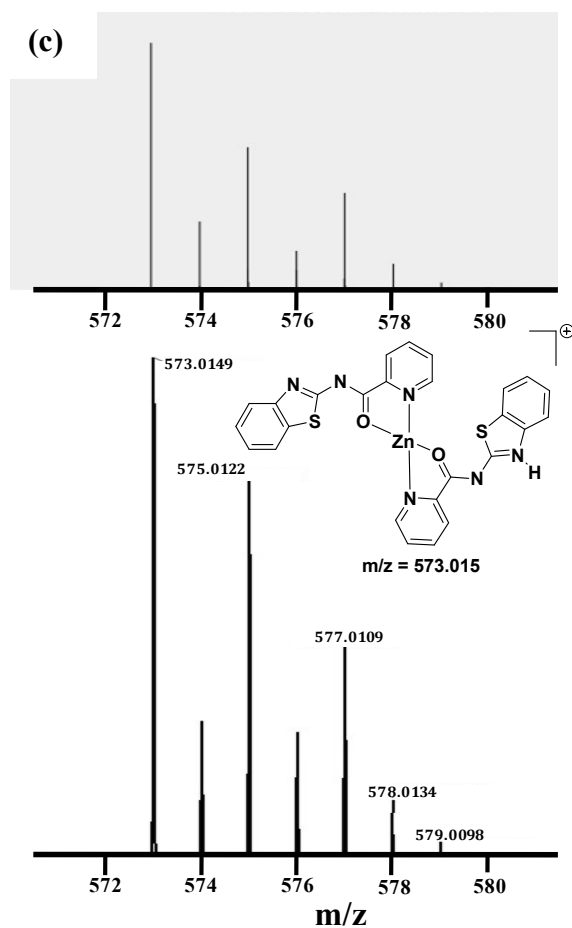
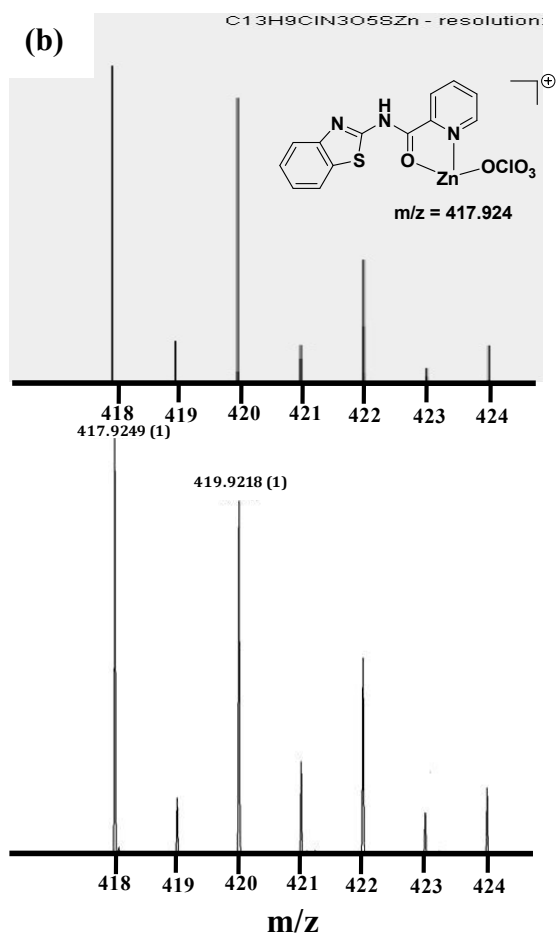
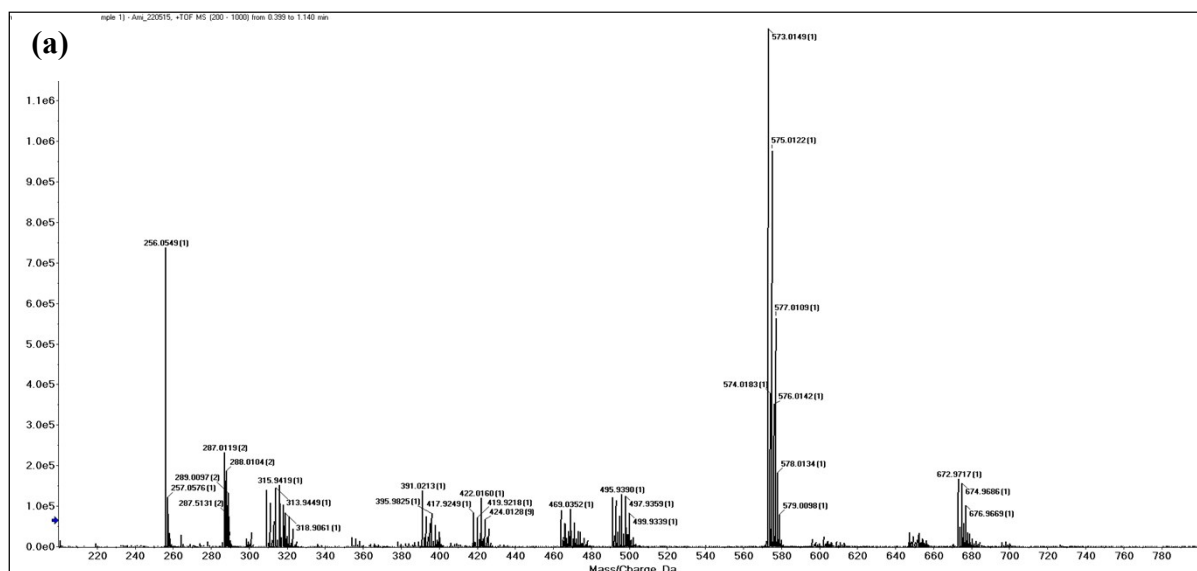


Figure S20. (a) Full range mass spectrum of Zn(II) complex **4-Zn** recorded in THF. (b and c) Comparison of relevant molecular ion peaks with the simulated ones. Simulated patterns were obtained from the online chemical calculator (Institute of chemical sciences and engineering).

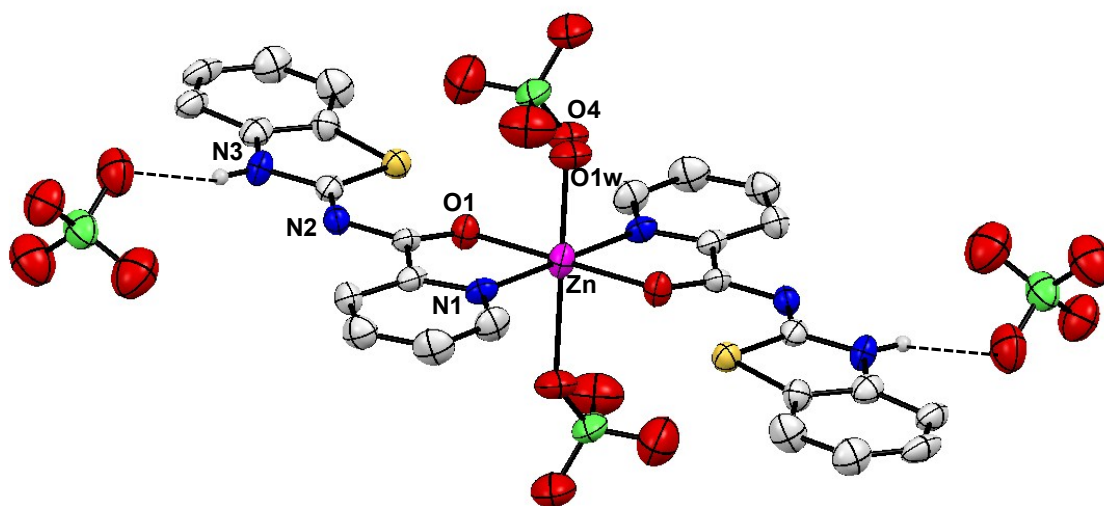


Figure S21. Thermal ellipsoidal representation of the crystal structure of **4-Zn[#]**; thermal ellipsoids are drawn at 30% level whereas all hydrogen atoms except those involved in hydrogen bonding have been omitted for clarity.

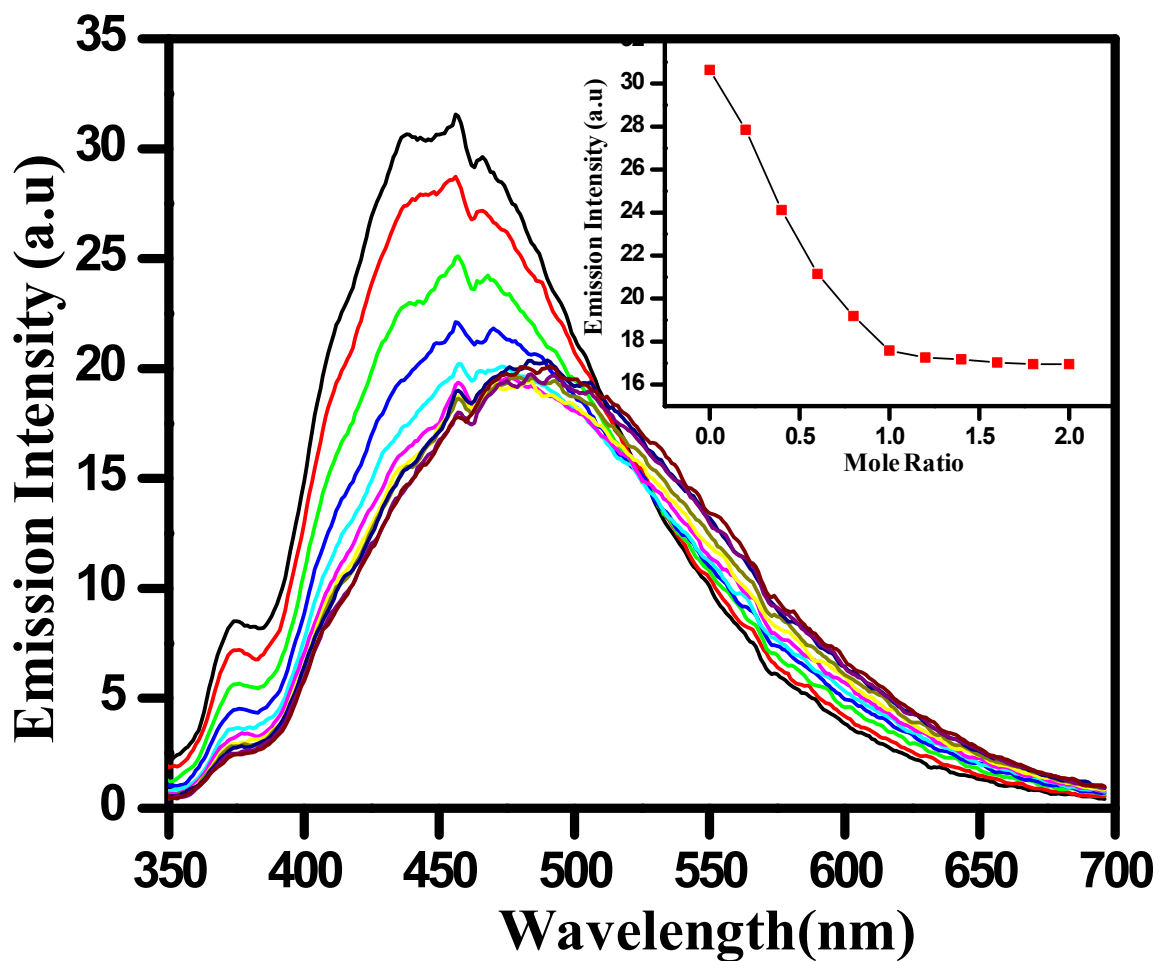


Figure S22. Change in the emission intensity of chemosensor 4 (0.1mM) with the increasing concentration of Zn(II) ion (0-0.2mM) in MeOH. Inset: Mole ratio plot exhibiting 1:1 stoichiometry between 4 and Zn(II) ion.

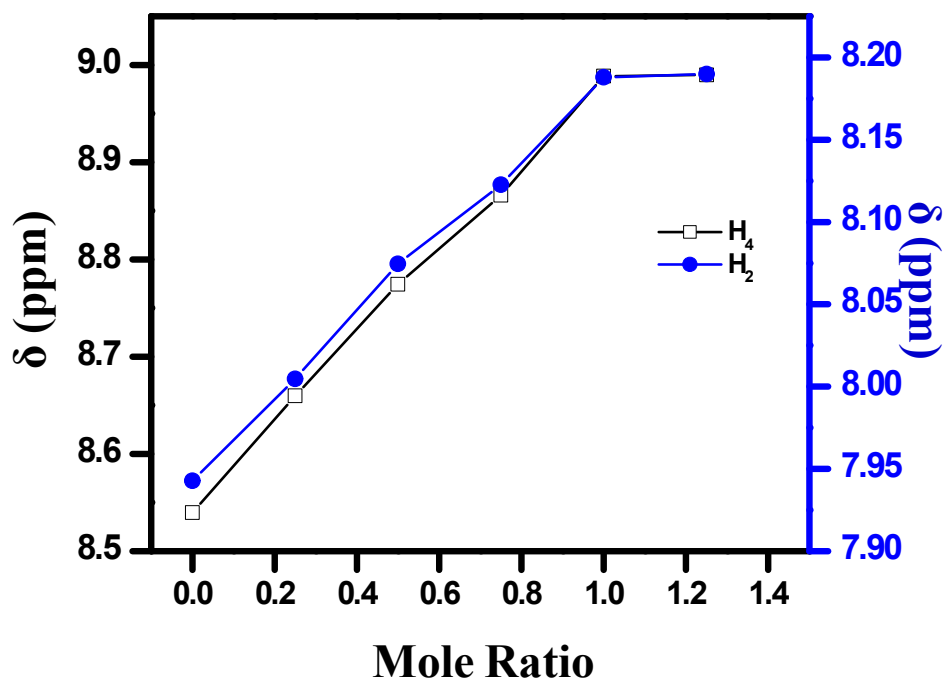
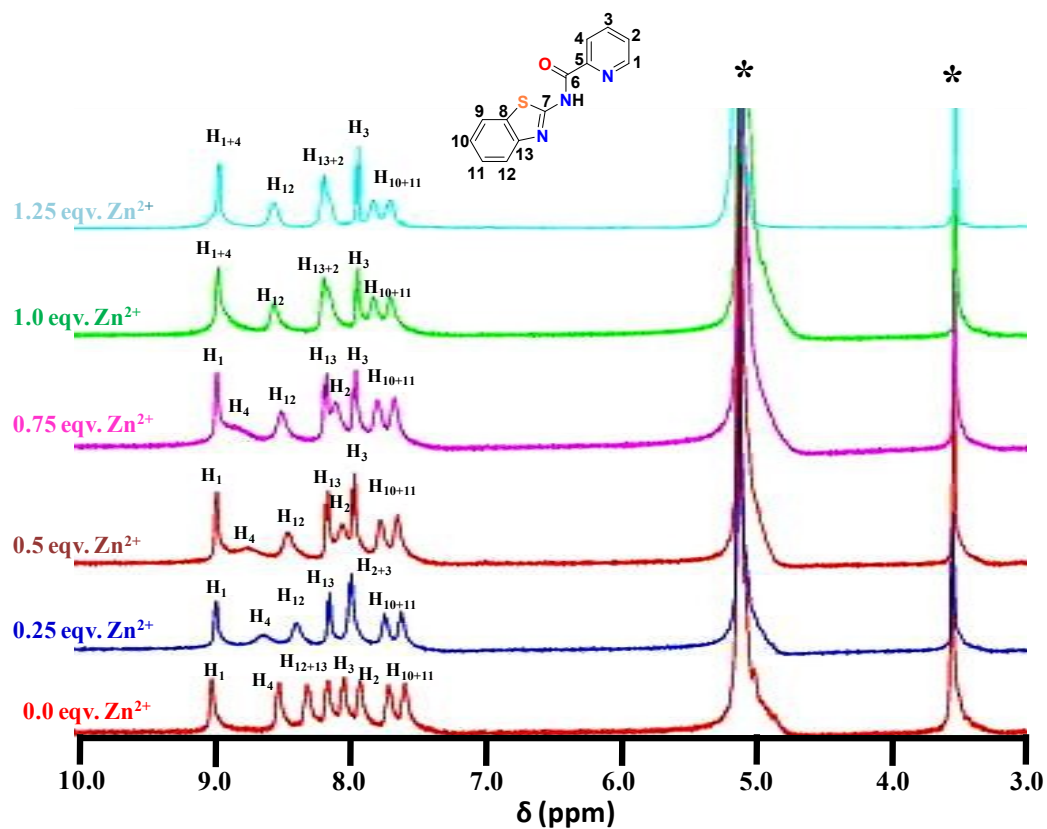


Figure S23. (above) ^1H NMR spectral titration of chemosensor **4** (1.0 mM) with increasing equivalents of $\text{Zn}(\text{II})$ ion (0-1.25 mM) in MeOH-d_4 . * Represents the residual solvent peaks. (below) Plot for the change in ^1H NMR chemical shifts of protons H_4 and H_2 with the increasing equivalents of $\text{Zn}(\text{II})$ ion.

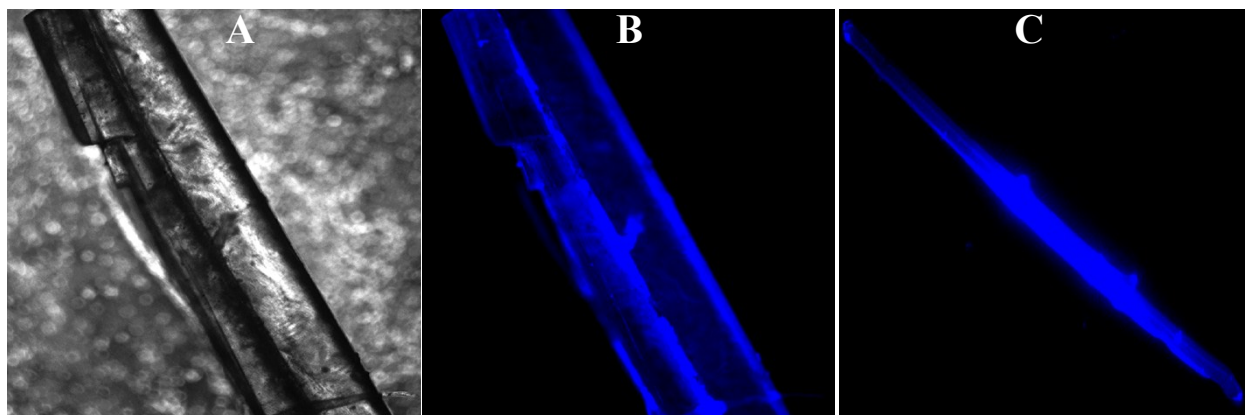


Figure 24. (A) Bright field microscopic image of a crystal of chemosensor **4**. (B)Fluorescent image of **4** under 330 nm UV-light. (c) Change in the emission of **4** after treating with Zn(II) ion solution (1 mM) in water for 5 min.

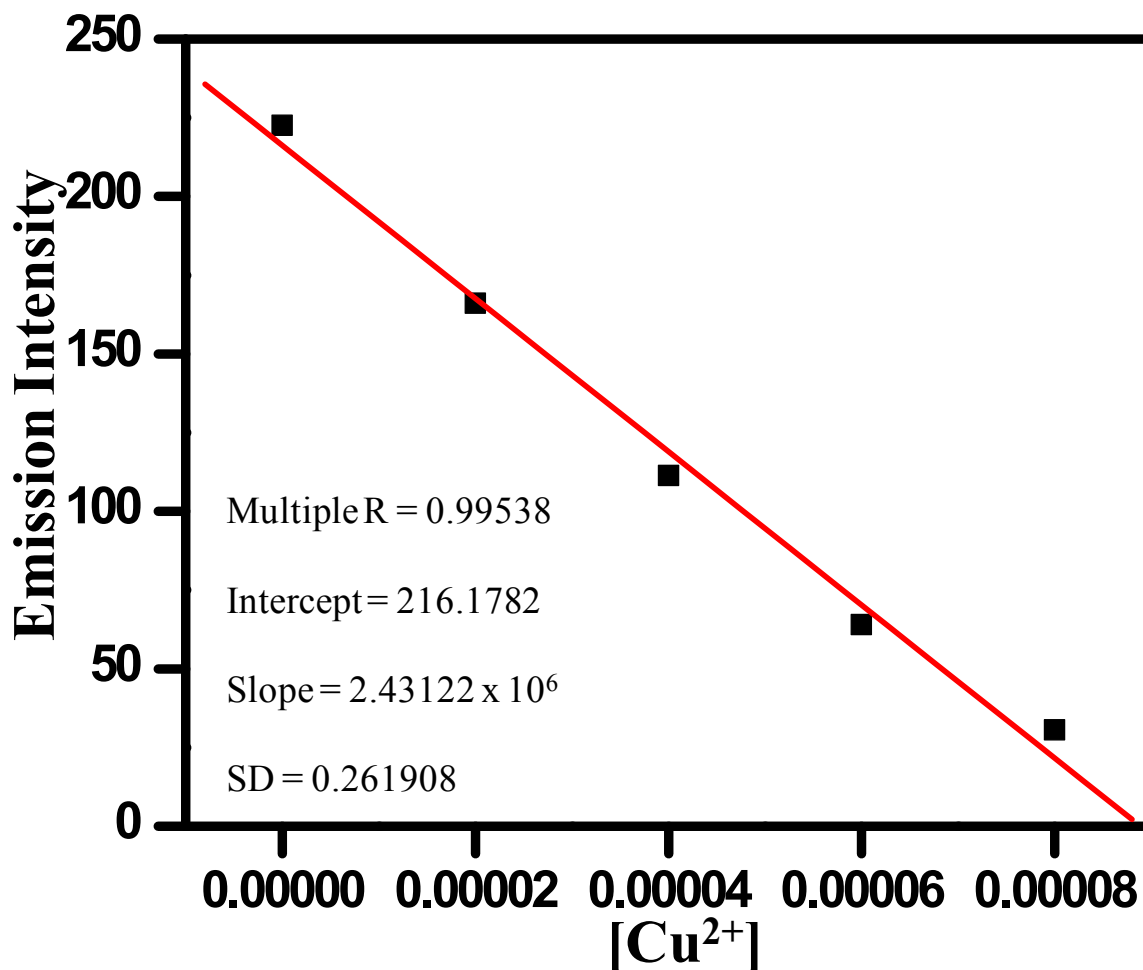


Figure S25. Calculation of detection limit for chemosensor **1**.

The detection limit was calculated based on the fluorescence titration. To determine the S/N ratio, the emission intensity of **1** without Cu²⁺ ions was measured 10 times and the standard deviation of blank measurements was determined. The detection limit was then calculated with the following equation:

$$DL = 3 \times SD/S$$

Where SD is the standard deviation of the blank solution measured by 10 times; S is the slope of the calibration curve. From the graph we get slope (S) = 2.43122×10^{-6} , and SD value is 0.261908. Thus using the formula we get the Detection Limit (DL) = 29.614×10^{-8} M; *i.e.* chemosensor **1** can detect Cu(II) ion in this minimum concentration through fluorescence method.

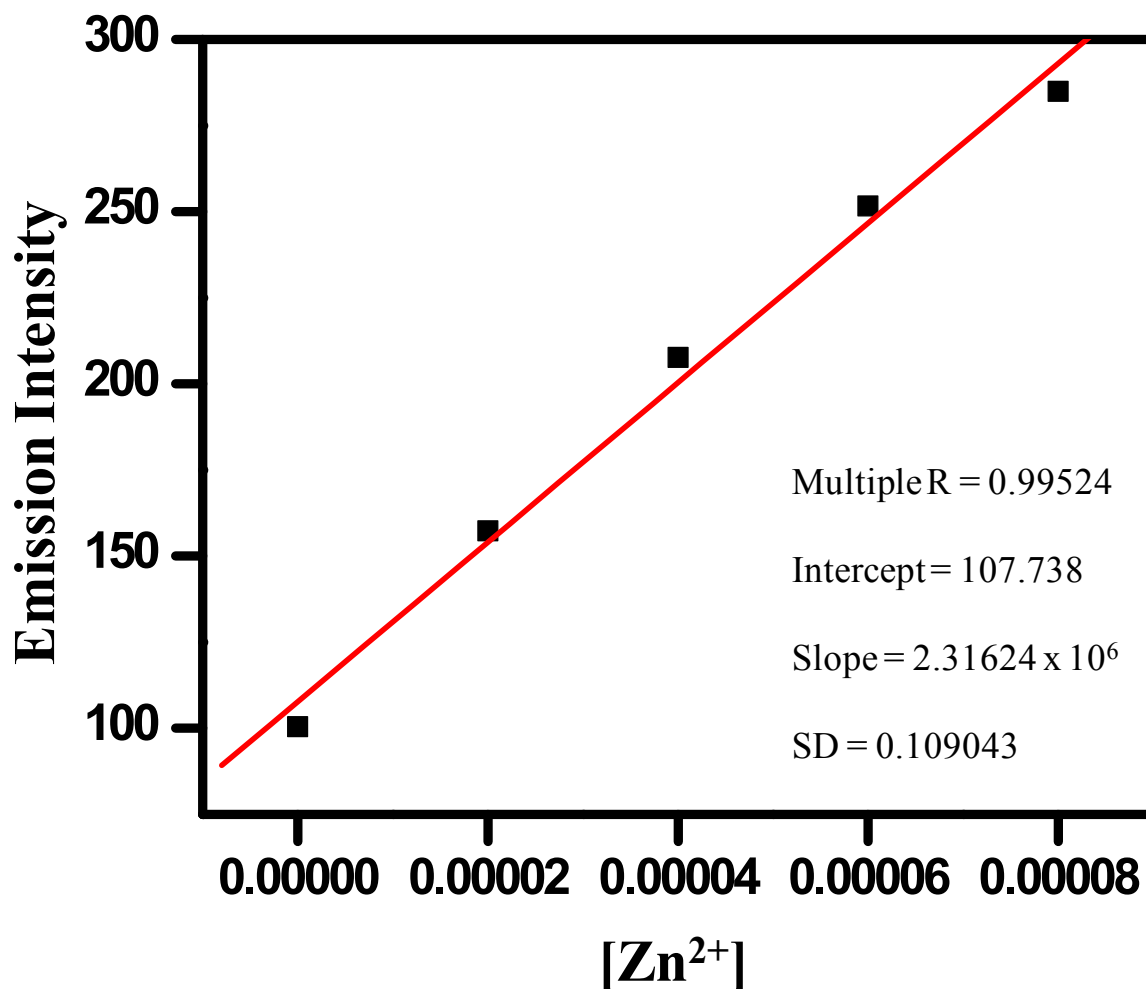


Figure S26. Calculation of detection limit for chemosensor 4.

The detection limit was calculated based on the fluorescence titration. To determine the S/N ratio, the emission intensity of 4 without Zn²⁺ ions was measured 10 times and the standard deviation of blank measurements was determined. The detection limit was then calculated with the following equation:

$$DL = 3 \times SD/S$$

Where SD is the standard deviation of the blank solution measured by 10 times; S is the slope of the calibration curve. From the graph we get slope (S) = 2.31624 x 10⁻⁶, and SD value is 0.109043. Thus using the formula we get the Detection Limit (DL) = 47.07 x 10⁻⁹ M; *i.e.* chemosensor 4 can detect Zn(II) ion in this minimum concentration through fluorescence method.

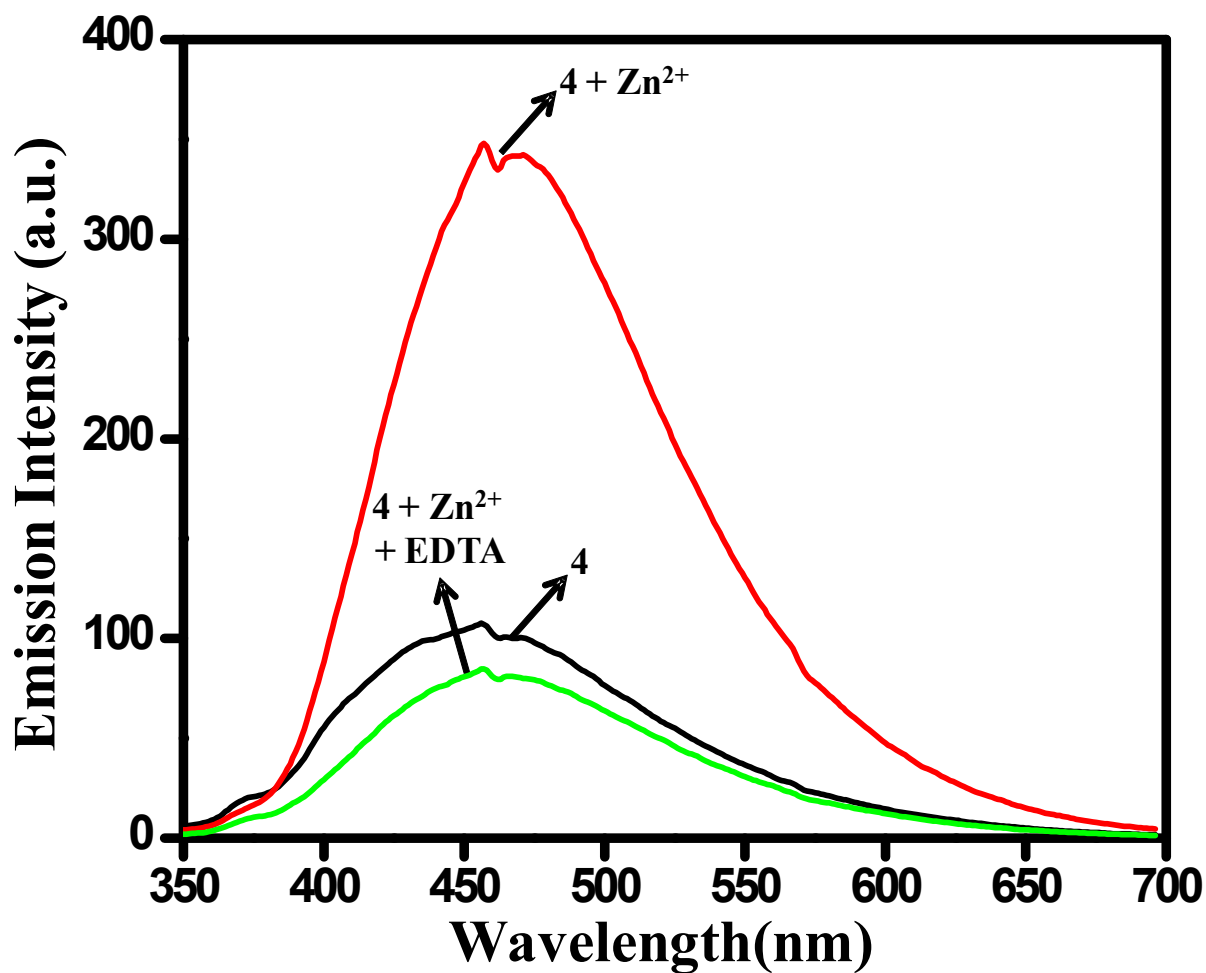


Figure S27. Recyclability experiment of chemosensor **4** (black trace); after the addition of one equiv. of Zn(II) ion (red trace); followed by the addition of one equiv. of Na₂EDTA (green trace).

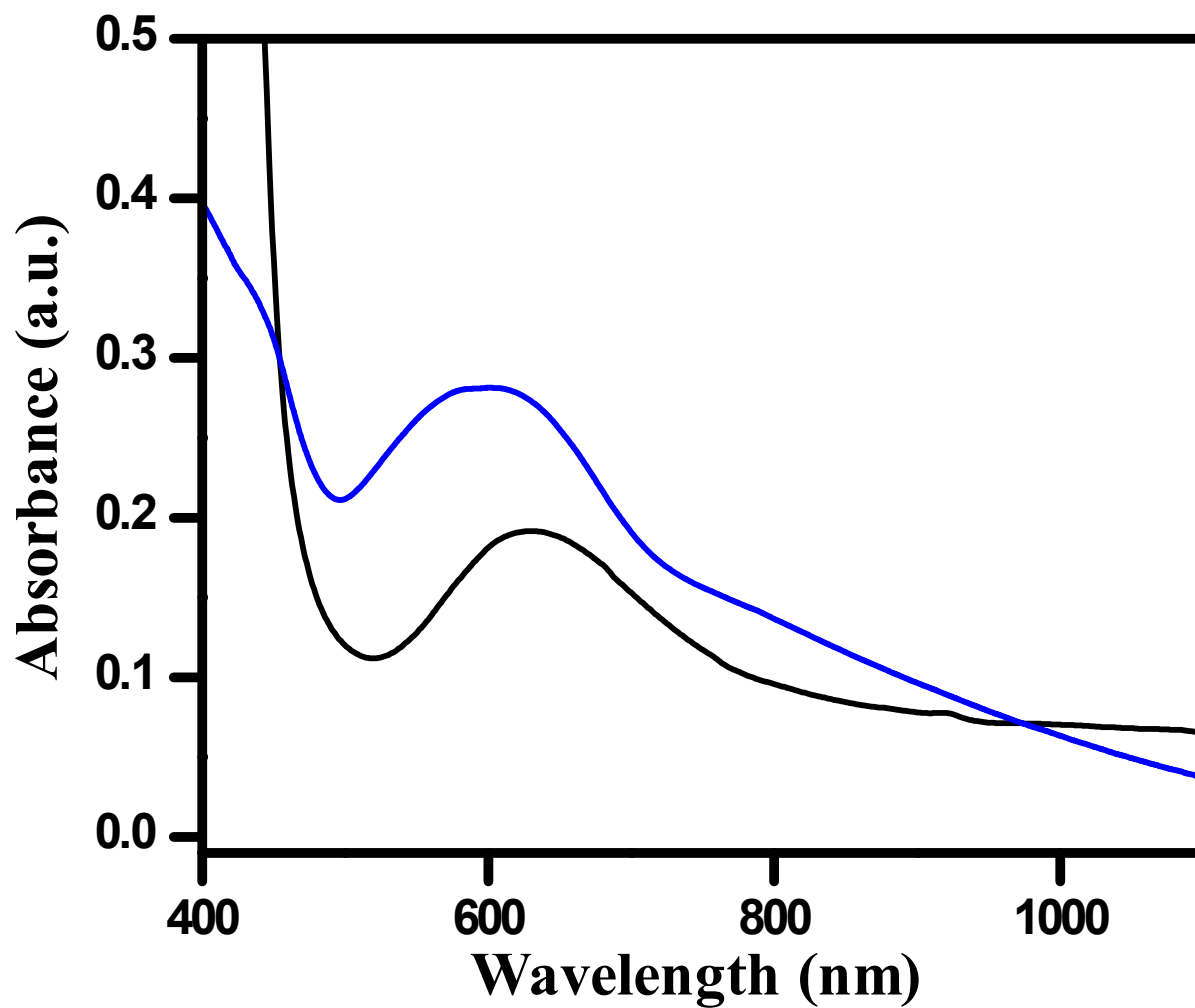


Figure S28. Solid-state diffuse reflectance absorption spectrum (blue trace) and THF solution absorption spectrum (black trace) of **1-Cu**.

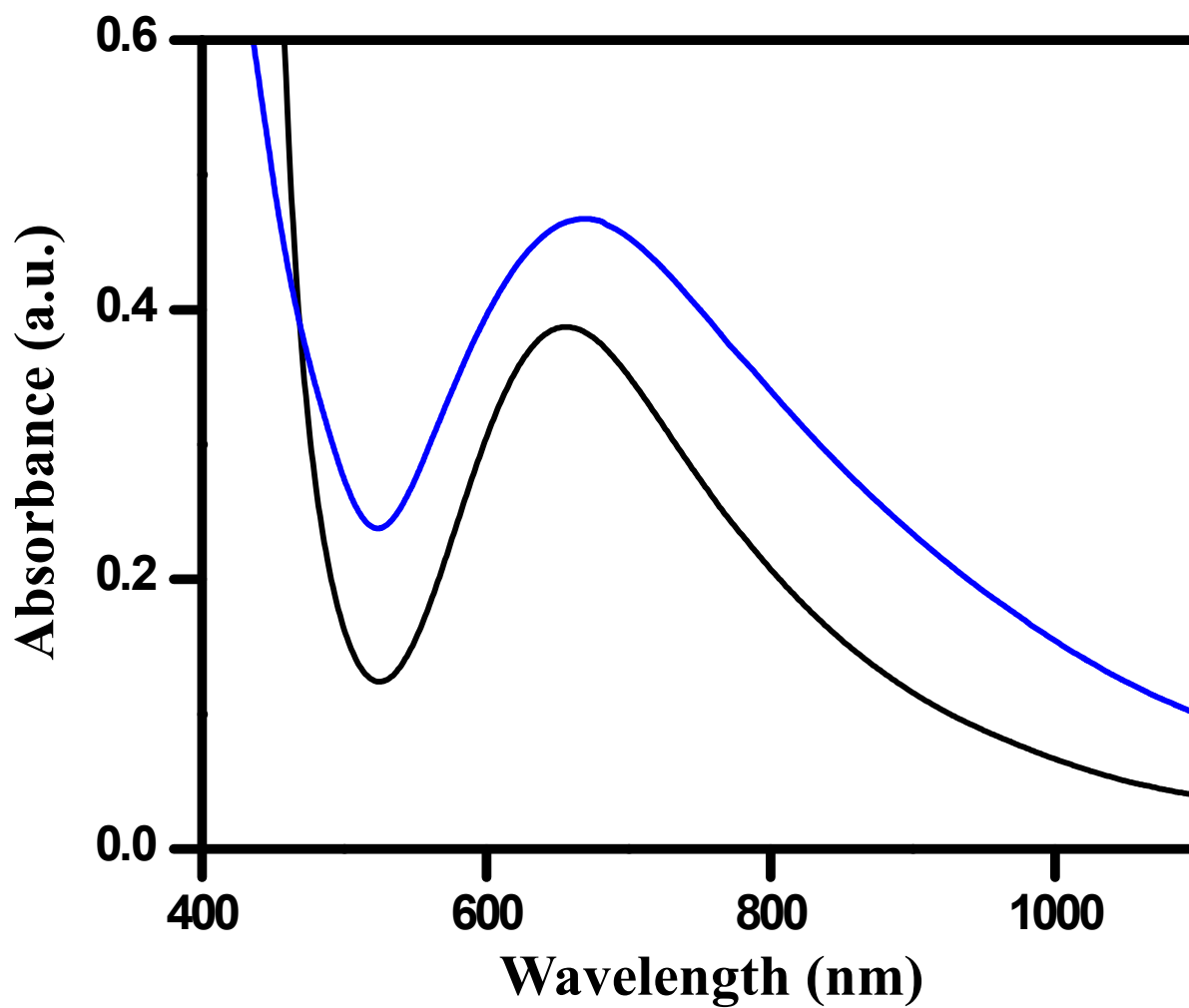


Figure S29. Absorption spectra of **1-Cu[#]**, in DMF (black traces) and diffuse reflectance (blue traces).

Table S1. Crystallographic data collection and structural refinement parameters for chemosensor **1** and **1-Cu[#]** and **4-Zn[#]**.

Compound	1•THF	1-Cu[#]•H₂O	4-Zn[#]•2H₂O
Formula	C ₂₅ H ₂₁ N ₅ O ₃ S ₂	C ₂₁ H ₁₃ CuN ₅ O ₃ S ₂	C ₂₆ H ₂₂ Cl ₂ N ₆ O ₁₂ S ₂ Zn
Formula weight	503.59	511.02	810.88
T (K)	293(2)	293(2)	293(2)
System	Monoclinic	Orthorhombic	Monoclinic
Space group	<i>P</i> 2 ₁ /c	<i>P</i> 2 ₁ 2 ₁ 2 ₁	<i>P</i> 2 ₁ /c
a (Å)	13.7363(14)	6.075(5)	12.145(5)
b (Å)	7.2021(5)	12.054(5)	7.935(5)
c (Å)	24.651(3)	26.823(5)	19.780(5)
α (°)	90	90	90
β (°)	98.952(10)	90	113.505(16)
γ (°)	90	90	90
V (Å ³)	2409.0 (4)	1964.2(18)	1748(14)
Z	4	4	2
ρ _{calc} (mg/m ³)	1.388	1.728	1.541
μ(mm ⁻¹)	0.259	1.362	1.041
<i>F</i> (000)	1048	1036	824
Goodness-of-fit (GOF) on F ²	0.968	1.106	1.156
Final R indices [<i>I</i> > 2σ(<i>I</i>)]	<i>R</i> ₁ = 0.0725, w <i>R</i> ₂ = 0.827	<i>R</i> ₁ = 0.0290, w <i>R</i> ₂ = 0.0722	<i>R</i> ₁ = 0.1232, w <i>R</i> ₂ = 0.3509
R indices (all data)	<i>R</i> ₁ = 0.1625, w <i>R</i> ₂ = 0.1079	<i>R</i> ₁ = 0.0307, w <i>R</i> ₂ = 0.0730	<i>R</i> ₁ = 0.1643, w <i>R</i> ₂ = 0.3608
CCDC No.	1425728	1425729	1425730

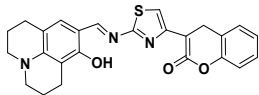
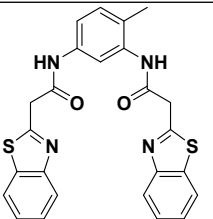
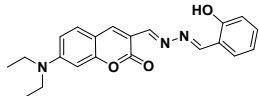
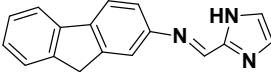
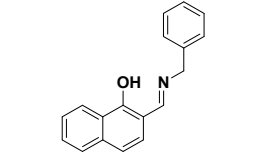
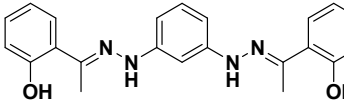
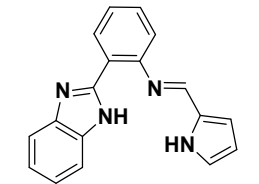
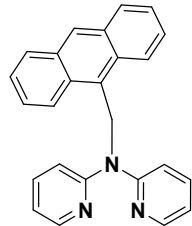
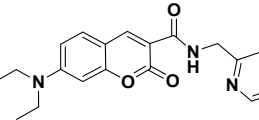
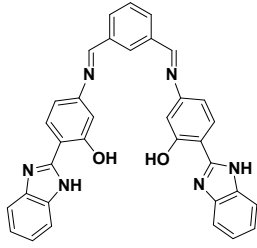
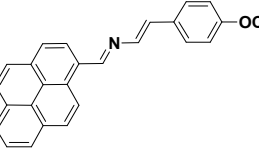
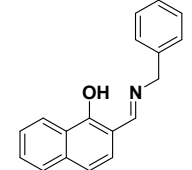
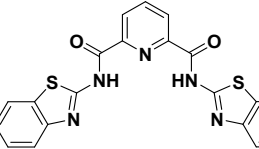
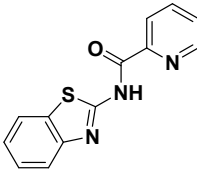
[a] $R_1 = \sum ||F_0| - |F_c|| / \sum |F_0|$; $wR_2 = \{ \sum [w(|F_0|^2 - |F_c|^2)^2] / \sum [wF_0^4] \}^{1/2}$.

Table S2. Selected bond distances (Å) and bond angles (°) for **1-Cu[#]** and **4-Zn[#]**.

Bonds	1-Cu[#]•H₂O	Bonds	4-Zn[#]
Cu-O1w	1.904(2)	Zn-N1	2.041(9)
Cu-N2	1.914(3)	Zn-O1	2.066(7)
Cu-N1	2.013(3)	Zn-O2	2.189(10)
Cu-N3	2.018(3)	N1-Zn-N1 ^{#1}	180.0
O1w-Cu-N2	176.46(12)	N1-Zn-O1 ^{#1}	99.8(3)
O1w-Cu-N1	99.20(11)	N1 ^{#1} -Zn-O1 ^{#1}	80.2(3)
N2-Cu-N1	80.95(11)	O1-Zn-O1 ^{#1}	180.0
O1w-Cu-N3	99.08(11)	N1-Zn-O2	87.5(5)
N2-Cu-N3	80.70(11)	N1 ^{#1} -Zn-O2	92.5(5)
N1-Cu-N3	161.64(10)	O1-Zn-O2	88.8(5)
----	----	O1 ^{#1} -Zn-O2	91.2(5)
----	----	N1-Zn-O2 ^{#1}	92.5(4)
----	----	N1 ^{#1} -Zn-O2 ^{#1}	87.5(5)
----	----	O2-Zn-O2 ^{#1}	180.0(9)

Symmetry transformations used to generate equivalent atoms: #1= 1-x,-y,-z+1

Table S3. A comparative table displaying the chemosensing abilities of assorted receptors reported in the literature along with chemosensors **1** and **4** (Present work).

S. No	Chemosensor	Cu ²⁺ Detection Limit (μM)	ref. no.	S. No	Chemosensor	Zn ²⁺ Detection Limit (μM)	ref. no.
1		1.53	7	8		0.67	13
2		0.27	8	9		10.0	14
3		0.82	9	10		0.69	15
4		0.98	10	11		2.06	16
5		0.5	11	12		3.0	17
6		4.58	12	13		0.35	9
7		0.29		14		0.047	

References.

1. D. D. Perrin, W. L. F. Armarego, D. R. Perrin, In *Purification of Laboratory Chemicals*, Pergamon Press, Oxford, UK, **1980**.
2. D. Bansal, G. Kumar, G. Hundal, R. Gupta, *Dalton Trans.* 2014, **43**, 14865.
3. *CrysAlisPro*, v. 1.171.33.49b, Oxford Diffraction Ltd., Abingdon, **2009**.
4. A. Altomare, G. Cascarano, C. Giacovazzo, A. Guagliardi, *J. Appl. Crystallogr.* 1993, **26**, 343.
5. G. M. Sheldrick, *Acta Crystallogr., Sect. A* 2008, **64**, 112.
6. L. J. Farrugia, WinGX, v. 1.70, An Integrated System of Windows Programs for the Solution, Refinement and Analysis of Single-Crystal X-ray Diffraction Data, Department of Chemistry, University of Glasgow, **2003**.
7. A. K. Mahapatra, S. Mondal, S. K. Manna, K. Maiti, R. Maji, M. R. Uddin, S. Mandal, D. Sarkar, T. K. Mondal and Dilip K. Maiti, *Dalton Trans.*, 2015, **44**, 6490.
8. J. -T. Yeh, W. -C. Chen, S. -R. Liu and S. -P. Wu, *New J. Chem.*, 2014, **38**, 4434.
9. A. Ganguly, B. K. Paul, S. Ghosh, S. Kar and N. Guchhait, *Analyst*, 2013, **138**, 6532.
10. P. Saluja, N. Kaur, N. Singh and D. O. Jang, *Tetrahedron Letters*, 2012, **53**, 3292.
11. H. S. Jung, P. S. Kwon, J. W. Lee, J. Kim, C. S. Hong, J. W. Kim, S. Yan, J. Y. Lee, J. H. Lee, T. Joo, J. S. Kim, *J. Am. Chem. Soc.*, 2009, **131**, 2008.
12. R. Martinez, F. Zapata, A. Caballero, A. Espinosa, A. Tarraga and P. Molina, *Org. Lett.*, 2006, **8**, 3235.
13. N. Khairnar, K. Tayade, S. K. Sahoo, B. Bondhopadhyay, A. Basu, J. Singh, N. Singh, V. Gite and A. Kuwar, *Dalton Trans.*, 2015, **44**, 2097.
14. A. Hens, A. Maity, K. K. Rajak, *Inorganica Chimica Acta*, 2014, **423**, 408.
15. S. S. Mati, S. Chall, S. Konar, S. Rakshit, S. C. Bhattacharya, *Sensors and Actuators B*, 2014, **201**, 204.
16. H. G. Lee, K. B. Kim, G. J. Park, Y. J. Na, H. Y. Jo, S. A. Lee, C. Kim, *Inorganic Chemistry Communications*, 2014, **39**, 61.
17. M. J. Kim, K. Kaur, N. Singh and D. O. Jang, *Tetrahedron*, 2012, **68**, 5429.